Monomers from vegetable oil feedstock: kinetics, catalysis and thermal risk
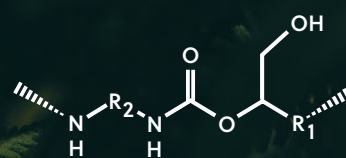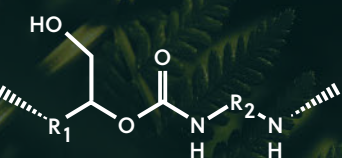
Wander Y. Pérez Sena

Åbo Akademi University
INSA Rouen Normandie
2021

Wander Y. Pérez Sena

Born 1992, Santo Domingo, Dominican Republic

M.Sc. Chemical Engineering, 2017
INSA – Rouen Normandie, France

Monomers from vegetable oil feedstock:
kinetics, catalysis and thermal risk

Monomers à base d'huiles vegétales:
cinétique, catalyse et risque thérmique

Monomerer från vegetabiliska oljor som råvara:
kinetik, katalys och termiska risker

Wander Y. Pérez Sena
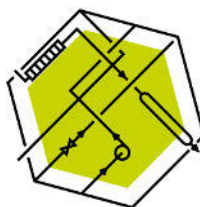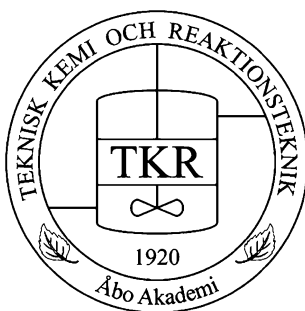
THESE

Pour obtenir le diplôme de doctorat

Spécialité Génie des Procédés

Préparée au sein de « l'Institut National des Sciences Appliquées de Rouen Normandie » et « Åbo Akademi University »

Monomers from vegetable oil feedstock: kinetics, catalysis and thermal risk

Présentée et soutenue par
Wander Y. Pérez Sena

Thèse soutenue publiquement le 9 juillet 2021 devant le jury composé de		
Riitta KEISKI	Professeure, Oulun yliopisto, Finlande	Rapporteure
Laurent FALK	Directeur de recherche CNRS, Université de Lorraine, France	Rapporteur
Tuomo SAINIO	Professeur, LUT-yliopisto, Finlande	Examinateur
Mélaz TAYAKOUT	Professeure, Université de Lyon, France	Examinatrice
Päivi MAKI-ARVELA	Professeure, Åbo Akademi, Finlande	Examinatrice
Lionel ESTEL	Professeur, LSPC, INSA Rouen, France	Co-Directeur de thèse
Tapio SALMI	Professeur académique, Åbo Akademi Finlande	Directeur de thèse
Sébastien LEVENEUR	MCF-HDR, LSPC, INSA Rouen, France	Directeur de thèse

Thèse dirigée par Sébastien LEVENEUR (INSA Rouen Normandie)
et Tapio SALMI (Åbo Akademi)

Dedicado a mi familia en Quisqueya la bella

"Let yourself be silently drawn by the strange pull of what you really love.

It will not lead you astray"

~Rumi

Preface

Five years have flown away since the day I left the comfort of my motherland in the Greater Antilles archipelago. With nothing in one hand and less in the other, very little I knew of what was ahead. La France was the destination, and the goal to make a better professional of me. Along my journey I stood on the shoulders of giants, leaders and friends whose support made possible this work and the product of it (a new doctor).

The best of my gratitude goes to Professor Sebastien Leveneur who unfolded the vast multiverse of chemical engineering before me, and helped me to take my first steps into the very exciting world of reaction engineering. Thank you for the tireless work and commitment.

The phrase 'thank you' is not enough to express my deep gratitude to academic Professor Tapio Salmi who has supported me as a mentor and a friend during this journey. I am deeply thankful for your guidance, for all those fruitful scientific and non-scientific discussions and for always believing in me. You are one of the most colorful person I have ever met, whose fervent passion for science is the fuel that keeps us, the young scientists, motivated.

It has been an honor for me to be advised by Professor Dmitry Murzin. Thank you for sharing your knowledge and your pure-gold lessons, you are indeed an unlimited source of inspiration.

I would like to thank Professor Lionel Estel for his support as a supervisor and for the nice mist that always surrounds his presence which made me feel at ease in every work meeting and discussion.

My gratitude and acknowledgment goes to my former supervisor Xiaoshuang Cai, who taught me the savoir-faires of the laboratory, thank you.

The absolute most needed person in this work was Kari Eränen, who has a solution for everything, when my experimental world failed, he always rescued it, thank you. In the same line I express my gratitude to Bruno Daronat and Sylvie Poubelle at LSPC, your technical support made possible the development of my project.

Thanks to Professor Johan Wärnå for the lessons in mathematical modelling, undoubtedly one of the most useful skill a chemical engineer can learn. Also, my thanks to Professor Narendra Kumar for the advice in catalyst synthesis.

I want to thank all of my colleagues and friends who made the PhD life more enjoyable during these years; Lu, Sanjuan, Wilson, Elizabeth, Orelso, Adriana, Ananias, Cesar, Liliveth, Henrik, Pasi, Atte, Päivi, Ole, Matias, Sebastian, JP, Nemanja, Jose, Mouad, Zuzana, Christoph, Mark, Jogi and the rest of my co-workers at the laboratories LSPC and TKR.

I want to specially thank Reetta Pekkinen for the support, and for being by my side in the happiest moments of the PhD Life.

Last but not least, all of this would have not been achievable without the unconditional support of my family to whom I dedicate this work. To my sisters; Yamile, Naylan and Raisi, with the hope my work serves as an inspiration, and to my parents; 'el Mello' and 'Colasa' who built the foundations of my education.

Abstract

Polyurethanes are among the most important polymers in our everyday life, they are industrially produced via the reaction of polyols and di-isocyanates. This process present multiple severe drawbacks such as high toxicity of the di-isocyanates. Furthermore, di-isocyanates are produced from petroleum-derived compounds such as phosgene, which is known to be an extremely toxic compound. In recent decades, a more environmental friendly strategy for the production of this precious polymer has emerged, that is the polymerization reaction of polycarbonates and polyamines, which takes the advantages of bio-based and carbon dioxide feedstock.

This scientific effort is devoted to the study of the reaction pathway for the production of polyurethanes from vegetable oils based raw materials. Vegetable oils are a green source of raw materials that offer several benefits such as non-toxicity, renewable character and biodegradable products.

Each reaction step required to upgrade vegetable oils to polyurethanes was investigated separately. The epoxidation reaction was first investigated from a process safety point of view. Different epoxidation methods were compared and it was found that direct epoxidation with hydrogen peroxide in the presence of a metal oxide catalyst such as aluminium oxide gives the lowest probability of thermal runaway. Thereafter, the kinetics of the system was investigated and its efficiency was enhanced by application of semi-batch reactor technology. Mathematical modelling of the reaction system was performed, and a rather good description of the experimental data was achieved.

A series of heterogeneous catalysts were synthetized and tested in the carbonation process of epoxidized vegetable oils. The most important parameter to obtain a good reactant conversion and product yield was the utilization of mesoporous materials as supports and the presence of a Lewis acidity source such as a metal.

A Tian-Calvet isothermal calorimeter was used to determine the reaction enthalpies of the aminolysis system. The reaction enthalpies of aminolysis and amidation were determined, denoting a low exothermicity. Thereafter, the kinetics of the aminolysis system was explored using four amines; mathematical models for each amine system were developed, and a linear free energy relationship (LFER) was established linking the substituent of the amine and the estimated reaction rate.

Referat

Polyuretaner hör till de viktigaste polymererna i vårt vardagliga liv; de framställs industriellt genom en reaktion mellan polyoler och diisocyanater. Denna process har flera allvarliga nackdelar, speciellt diisocyanaternas höga giftighet. Dessutom framställs isocyanater ur petroleumbaserade komponenter som fosgen, som är en synnerligen giftig molekyl. Under de senaste årtiondena har en miljövänligare produktionsstrategi för denna värdefulla polymer utvecklats, dvs polymerisationsreaktioner mellan polykarbonater och polyaminer. Processen utnyttjar fördelarna med biobaserad råvara och koldioxid.

Detta vetenskapliga arbete fokuserar på studier av miljövänliga reaktionsvägar för produktion av polyuretaner ur råvaror som härstammar från växtoljor. Växtoljorna utgör en grön källa av råmaterial med flera fördelar: de är giftfria, förnyelsebara och reaktionsprodukterna är biologiskt nedbrytbara.

Varje reaktionssteg som behövs för att uppgradera växtoljor till polyuretaner studerades separat. Epoxideringsprocessen undersöktes först ur processäkerhetens synvinkel. Olika epoxiderings-metoder jämfördes och resultaten visade att direkt epoxidering med väteperoxid i närvaro av en metalloxidkatalysator, t.ex. aluminiumoxid har den lägsta sannolikheten för en okontrollererad temperaturstegring. Därefter kartlades systemets kinetik och processens effektivitet förbättrades genom att tillämpa halvkontinuerlig drift. Reaktionssystemet modellerades matematiskt och experimentella data kunde relativt väl beskrivas med hjälp av modellen.

Flera heterogena katalysatorer syntetiserades och testades i karbonering av epoxiderade växtoljor. De viktigaste parametrarna för att uppnå en god reaktantomsättning och produktutbyte var utnyttjandet av porösa material som bärare samt närvaron av en Lewissyrakälla, t.ex. en metall.

En isotermisk Tian-Calvetkalorimeter användes för att mäta reaktionsentalpierna för aminolyssystemet. Reaktionsentalpierna för aminolys och amidering bestämdes och de indikerade en svag exotermicitet. Därefter studerades kinetiken av aminolyssystemet genom att använda fyra olika aminer; matematiska modeller för varje aminsystem utvecklades och relationer baserade på linjär fri energi utnyttjades för att bekräfta sambandet mellan aminsubstituenten och den estimerade reaktionshastigheten.

Résumé

Les polyuréthanes se trouvent parmi les plus importants polymères de la vie quotidienne, ils sont produits au niveau industriel par la réaction entre un polyol et un diisocyanate. Ce procédé présente plusieurs inconvénients comme la toxicité du diisocyanate. Ces deniers sont obtenus à partir de dérivés de pétrole comme le phosgène, lequel est connu par sa haute toxicité. Dans ces dernières années, une nouvelle voie de synthèse plus respectueuse de l'environnement pour la production de cet important polymère a été développée, il s'agit de la réaction de polyaddition entre un polycarbonate et une polyamine, ce procédé utilise des biosources et dioxyde de carbone comme matières premières.

Le présent travail scientifique est consacré à l'étude du chemin réactionnel pour la production de polyuréthanes à partir des huiles végétales comme matières premières. Les huiles végétales sont une source verte des matériaux qui offrent plusieurs avantages comme ; non toxicité, renouvelables et biodégradabilité des produits finals.

Chaque étape réactionnelle nécessaire pour transformer des huiles végétales en polyuréthanes a été étudiée. La réaction d'époxidation a été d'abord évaluée d'un point de vue de sécurité de procédé. Diverses méthodes de synthèse des époxydes ont été comparées, et il a été trouvé que l'époxidation directe par le peroxyde d'hydrogène en présence d'un catalyseur oxyde métallique comme l'oxyde d'aluminium donne les plus basse probabilités d'emballement thermique. Ensuite, la cinétique du system a été étudiée, et le rendement a été amélioré par application de la technologie de réacteur semi-fermé. Modélisation mathématique du system réactionnel a été menée, et une bonne description des données expérimentales a été obtenue.

Une variété des catalyseurs hétérogènes ont été synthétisés et testés dans l'étape de carbonisation des huiles végétales époxydées. Les plus importants paramètres pour l'obtention des bonnes conversions et rendements ont été l'utilisation d'un matériau pésoporeux et la présence d'une source d'acidité de Lewis comme un métal.

Un calorimètre isothermique a été utilisé pour la détermination des enthalpies de réaction dans l'étape d'amynolyse. Les enthalpies de réaction de l'amynolyse et l'amidation ont été trouvées légèrement exothermiques. Par la suite, la cinétique du system a été étudié en utilisant quatre amine différentes ; des modèles mathématiques pour chaque system ont développées et une relation d'énergie libre a été établie en liant le substituent des amines et leurs contant cinétiques.

Resumen

El poliuretano es uno de los polímeros más importantes de nuestra vida cotidiana, el cual es producido industrialmente atreves de la reacción entre polioles y diisocianatos. Este proceso presenta varios inconvenientes como es la toxicidad del disocianato. Este es obtenido de compuestos derivados de petróleo como el fosgeno, el cual es conocido por ser extremadamente toxico. En pasadas décadas, han surgido nuevas tecnologías para la producción de este importante polímero tomando en cuenta el cuidado del medio ambiente, la polimerización entre policarbonatos y poliaminas, es un claro ejemplo de esto, la cual aprovecha recursos naturales y dióxido de carbonos como materia prima.

Este trabajo científico se enfoca en el estudio de la vía de producción de poliuretano a partir de aceites vegetales como materia prima. Los aceites vegetales son una fuente verde de materiales que ofrece múltiples beneficios; no son toxicos, son renovables y los productos que generan son biodegradables.

Cada etapa de reacción necesaria para convertir aceites vegetales en poliuretano fue investigada. La reacción de epoxidación fue primero investigada desde un punto de vista de seguridad de procesos. Diferentes métodos de epoxidación fueron comparados, y se encontró que la epoxidación directa con peróxido de hidrógeno en la presencia de un oxido metálico como el óxido de aluminio resulta en las menores probabilidades de explosión térmica. Luego, la cinética del sistema fue investigada y su rendimiento fue mejorado por aplicación de tecnología de reactor semi-continuo. Modelización matemática del sistema de reacción fue llevado a cabo, y una buena descripción de los datos experimentales fue obtenida.

Varios catalizadores heterogéneos fueron sintetizados y evaluados en el proceso de carbonización. Los parámetros más importantes para obtener buenas conversiones y rendimientos de producto, fueron la utilización de materiales mesoporosos y la presencia de una fuente de acidez de Lewis como por ejemplo un metal.

Las entalpias de reacción del sistema de aminolisis fueron determinadas en un calorímetro isotérmico. Las reacciones de aminolisis y amidación fueron encontradas levemente exotérmicas. Luego, la cinética del sistema fue explorada usando cuatro diferentes aminas; modelos matemáticos para cada sistema fueron desarrollados, y una expresión lineal de energía libre fue establecida relacionando el sustituyente de la amina y la velocidad de reacción.

x

List of publications

I.   **W. Y. Pérez-Sena**, X. Cai, N. Kebir, L. Vernières-Hassimi, C. Serra, T. Salimi, S. Leveneur, 'Aminolysis of cyclic-carbonate vegetable oils as a non-isocyanate route for the synthesis of polyurethane: A kinetic and thermal study'*, Chemical Engineering Journal*, 346 (2018) 271–280

II.   **W. Y. Pérez-Sena**, T. Salmi, L. Estel, and S. Leveneur, 'Thermal risk assessment for the epoxidation of linseed oil by classical Prisleschajew epoxidation and by direct epoxidation by H_2O_2 on alumina', *Journal of Thermal Analysis and Calorimetry*, 140(2) (2020) 673–684

III.   F. Guzmán Agudelo, **W. Y. Pérez-Sena**, N. Kebir, T. Salmi, L. A. Ríos, and S. Leveneur, 'Influence of steric effects on the kinetics of cyclic-carbonate vegetable oils aminolysis', *Chemical Engineering Science*, 228 (2020) 115954

IV.   **W. Y. Pérez-Sena**, J. Wärnå, K. Eranen, P. Tolvanen, L. Estel, S. Leveneur, T. Salmi, 'Use of semibatch reactor technology for the investigation of reaction mechanism and kinetics: Heterogeneously catalyzed epoxidation of fatty acid esters', *Chemical Engineering Science*, 230 (2021) 116206

V.   **W. Y. Pérez-Sena**, K. Eranen, N. Kumar, L. Estel, S. Leveneur, T. Salmi, 'New insights into the carbonation of epoxidized methyl oleate using single-component heterogeneous catalysts', (Submitted)

Wander Y. Pérez Sena's contribution to articles I-V

I, II, IV, V: Investigation, methodology and writing.

IV: Investigation and methodology.

Conference publications related to the topic

I. **W. Y. Pérez-Sena**, X. Cai, N. Kebir, L. Vernières-Hassimi, C. Serra, T. Salimi, S. Leveneur, Development of a kinetic model for polyurethanization from carbonated vegetable oils, 5th International Conference on Chemical Reaction Engineering (ISCRE), May 2018, Florence, Italy. – *Poster presentation*

II. **W. Y. Pérez-Sena**, T. Salmi, L. Estel, and S. Leveneur, Direct epoxidation of linseed oil by hydrogen peroxide: Thermal risk assessment, 12th European Congress of Chemical Engineering (ECCE), September 2019, Florence, Italy. – *Oral presentation*

III. **W. Y. Pérez-Sena**, J. Wärnå, K. Eranen, P. Tolvanen, L. Estel, S. Leveneur, T. Salmi Semibatch technology improves the direct epoxidation of fatty acid esters, 24th International Congress of Chemical and Process Engineering (CHISA), March 2021, Prague, Czech Republic. – *Oral presentation*

IV. **W. Y. Pérez-Sena**, J. Wärnå, K. Eranen, P. Tolvanen, L. Estel, S. Leveneur, T. Salmi Kinetic modelling of the alumina catalyzed epoxidation of fatty acid esters in a batch reactor, 11th International Symposium on Catalysis in Multiphase Reactor (CAMURE), March 2021, Milan, Italy. – *Oral presentation*

Table of content

1. Introduction

1.1 Biomass

The utilization of biomass as a source of raw materials for the production of energy and chemicals is a promising field of research. In recent years, many new technologies featuring biomass derived-feedstock have emerged in academic and industrial sectors. The main motivation in the utilization of biomass is the presumable depletion of fossil resources, as also the environmental pollution associated to production of fossil derived materials, chemicals and energy. Biomass derived feedstock on the other hand, is an environmentally-friendly resource that can contribute to the mitigation of those issues. Renewable resources and biodegradable products are the key advantages of biomass utilization, as well as carbon neutrality of the bio-based raw materials, which provides our society with a different perspective for a more sustainable life.

Biomass, more specifically plant-based biomass is composed of cellulose, lignin, hemicelluloses and extractives. The extractive fraction represent about 5wt% of biomass and consists of nonstructural components that can be extracted by means of solvents, some examples are; oils, fats, waxes, proteins, terpenes, phenolic compounds and simple sugars [1]. In recent years, extensive research has been conducted on the utilization of those components raw-materials. Components from biomass can be transformed to final products through the concept of biorefinery, in which, biomass is firstly breakdown to its building block compounds and then further processed and converted into more valuable products , chemicals, energy and biofuels [2].

1.2 Vegetables oils as a green feedstock

Among the extractive fraction of biomass, natural oils and fats are resources with a great potential for the production of variety of chemicals and products such as biofuels, pharmaceuticals, alimentary products, lubricants and polymers. Within this class, vegetable oils represent attractive biomass components, because of availability in large quantities and presence in almost every region of the globe. Furthermore, vegetable oils are a versatile feedstock that can be valorized through several reactions such as hydrogenation, transesterification, aminolysis, oxidation and epoxidation.

Despite arising concern on the utilization of vegetable oils and their competition with the alimentary sector, many non-edible oils are available for transformation and upgrading. On the other hand, the utilization of large areas for the plantation of agricultural crops devoted to the exclusive production of non-edible oils is still in direct competition with food industry. One of the most suitable solution to this controversial issue is the utilization of residues from agricultural, forestry, wood, pulp and paper industries [3]. In fact, studies on the application of waste-based oils for the production of valuable products have already been reported. Tall oil is an example of this kind of bio-sourced oils, which is a by-product of the well-established Kraft process in cellulose production.

In general, vegetable oils are a complex mixture of triglycerides and free fatty acids which can be saturated, monounsaturated or polyunsaturated. Some of the most common fatty acids present in the majority of vegetable oils are oleic acid, linoleic acid, linolenic acid and stearic acid, but their proportion and their form (free or triglyceride-bonded) depends on the source of the vegetable oil. Typical molecules appearing in vegetable oils are illustrated in Figure 1.
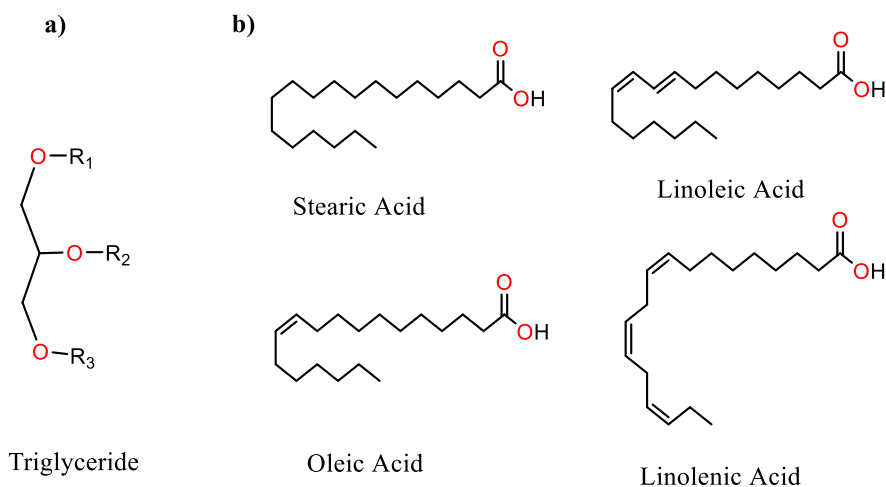
Figure 1. Example of vegetable oil; a) typical triglyceride molecule, where R_x is an alkyl chain of fatty acid b) common free fatty acids in vegetable oils.

Vegetable oils and their derivatives are important organic platform molecules for the synthesis of wide array of products. Valuable epoxides can be made by reacting vegetable oils with hydrogen peroxide. The conversion of the double bond functional groups of the vegetable oils to epoxides is typically conducted using hydrogen peroxide as the oxidizing agent of preference,

since it is a rather inexpensive and environmentally benign compound that decomposes into water and oxygen.

Functionalization to epoxides is a very attractive route because of the versatility of the epoxides for further transformations. They can be upgraded to other products of significant interest, for example to polyols, polyether, polyester and polycarbonate (Figure 2). Among these, polycarbonate are a class of compounds with relevant industrial applications as polymers precursors, fuel additives and solvents [4]. Moreover, this transformation involves the utilization of carbon dioxide and therefore contributes to some extent to the utilization of this greenhouse gas (GHG).
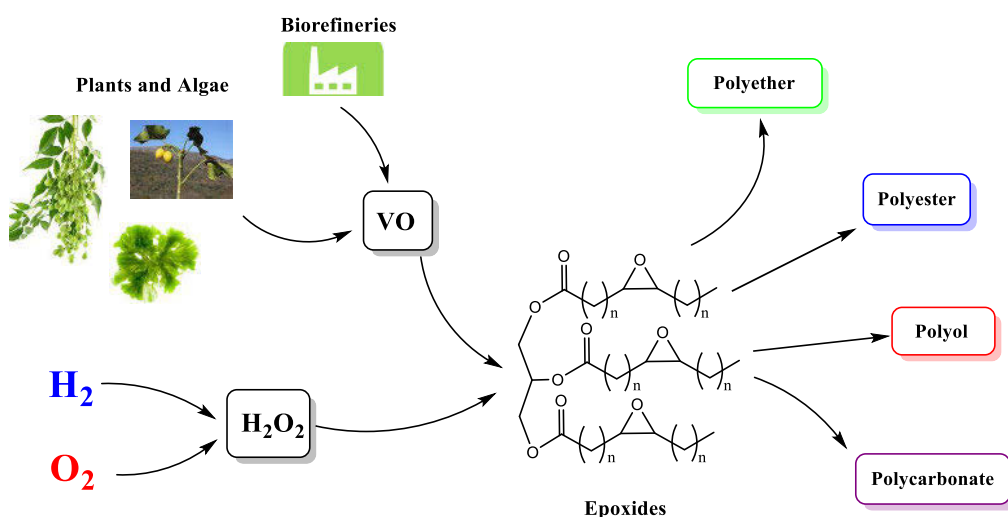
Figure 2. Epoxides from vegetable oil (VO) and derived products.

1.3 CO$_2$ as a C1 building block

The main driving forces for the biorefinery implementation are climate change and sustainable production of materials and energy. The greenhouse gas (GHG) emissions and their impact on global warming have been a motive of concern in the past decades, carbon dioxide figuring as one the principal greenhouse gases responsible for climate change, particular attention have been dedicated to the development of technologies that could help to reduce the emissions of GHG.

Carbon dioxide sequestration is one of the main approaches to partially keep CO_2 emissions controlled by avoiding the release of CO_2 produced in power plants to the atmosphere. Some of the used technologies for capturing CO_2 are post-combustion, precombustion, oxy-combustion, and chemical looping combustion [5]. Valorization of CO_2 is the second stage of this mitigation strategy, captured CO_2 can be valorized through three different routes; no transformation route, in which CO_2 is reused directly or used to assist in a process (e.g. hydrocarbon recovery), biologic transformation route, using technologies such as microalgae and biocatalysis and lastly chemical transformation route in which carbon dioxide is converted via chemical reactions into products such as fine chemicals and polymers [6] (see Figure 3) .
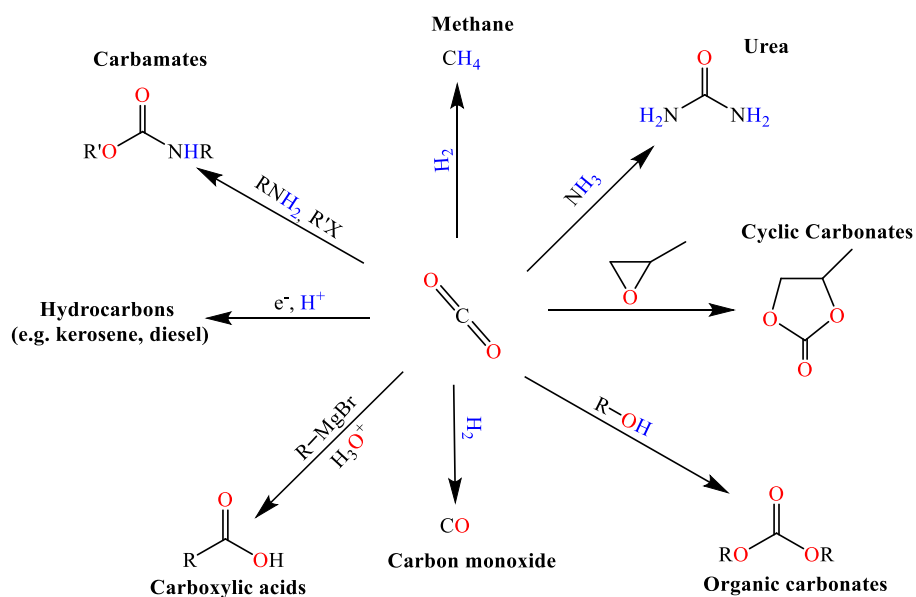
Figure 3. Summarized carbon dioxide coupling reactions and derived chemicals.

The chemical transformation routes of CO_2 offer many attractive and chemically exciting directions, among those the cycloaddition reaction to epoxides is a particularly interesting one. By synergistically using biomass-derived feedstock in conjunction with CO_2, new platform molecules are produced bearing the benefits of both technologies: the molecules are obtained from renewable resources, they are biodegradables and at the same time contribute to the mitigation of GHG emissions to the atmosphere. Cyclic carbonates produced from CO_2 and biobased feedstock are attractive molecules that find applications as aprotic solvents and intermediates for a variety of chemicals and polymers. In fact, their utilization for the

production of polyurethanes (the 6th ranked most produced polymer) is a field of research that has captured the attention of the scientific community, and in contrast with the classical and industrial polyurethanes production process this route avoids the use of petroleum-derived and toxic compounds.

1.4 Polyurethanes

Polyurethanes are a class of polymers present in a variety of forms in our everyday life. The market of polyurethanes includes medical, automotive, construction and other industrial sectors. The conventional process for the production of polyurethanes is based on the reaction between polyols and di-isocyanates. Polyurethanes are used to elaborate a wide spectrum of products, from furniture, coating, adhesive and elastomers to building materials and synthetic skins [7].
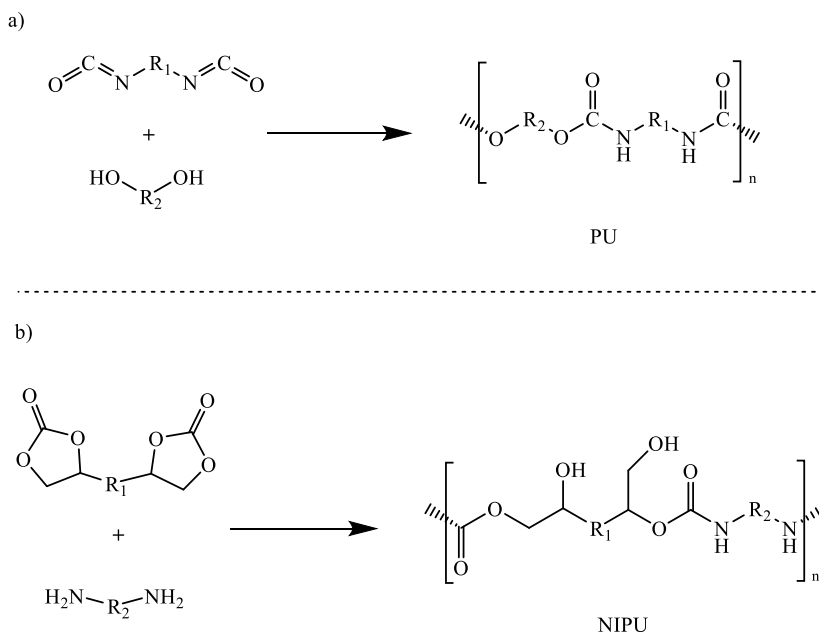
a)

b)

Figure 4. Polyurethane synthesis route; a) Conventional di-isocyanate route, b) Non-isocyanate route.

Something worth noting from the conventional process, is that di-isocyanates are toxic petroleum-derived compounds, which are very sensitive to moisture and require careful storage. Moreover, their phosgene precursors are extremely toxic as well and represent environmental

hazard. The production of these chemicals requires the utilization of specially designed equipment for their handling. Hence, a very challenging task in polymer science and technology have been the development of sustainable routes for the production of this very important polymer. An emerging route for the production of non-isocyanate polyurethanes (NIPUs) is the reaction of polycarbonates with polyamines to afford polyhydroxyurethane. Opposed to classical PU, NIPUs have shown improved organic solvent resistance due to the introduced OH functionalities, as well as higher tensile strength and a better thermal stability has been reported for polyurethanes obtained via the isocyanate-free route [8].

In line with this route, carbonated vegetables oils represent an attractive feedstock of polycarbonates for the production of NIPUs because of their renewable character and availability. Carbonated vegetable oils are typically obtained from epoxidized vegetable oils through cycloaddition reactions with carbon dioxide. Moreover, the epoxidized vegetable oil precursor can be easily synthetized by reacting the unsaturated vegetable oil with hydrogen peroxide. Hence, the necessary raw material for the non-isocyanate polyurethane route can be manufacture in a fairly green way.

Some research groups [6–10] have investigated the synthesis of NIPUs using cyclic carbonates derived from vegetables oils such as cottonseed, linseed and soybean oils. The obtained polymeric materials have been precisely characterized in terms of thermophysical and mechanical properties (e.g. mechanical strength and glass transition temperature), which are of special importance for thermoplastic elastomer and engineering applications. However, the kinetics of this reaction are scarcely explored in literature. In order to have a better understanding of the reaction and to possibly implement it at the industrial scale, kinetic studies aiming at determining the formation rate of polyurethane are the key issue.

The reaction strategy for the production of polyurethanes from vegetable oils feedstock is illustrated in Figure 5. At the first stage the vegetable oil (VO) of choice undergoes epoxidation reaction with hydrogen peroxide to yield epoxidized vegetable oil (EVO). Thereafter cyclic carbonates are produced via cycloaddition reaction using CO_2. The carbonated vegetable oil (CVO) bearing multiple carbonate groups is an ideal raw material for aminolysis reaction using di-amines (can also be obtained from bio-based feedstock) to produce polyurethanes.
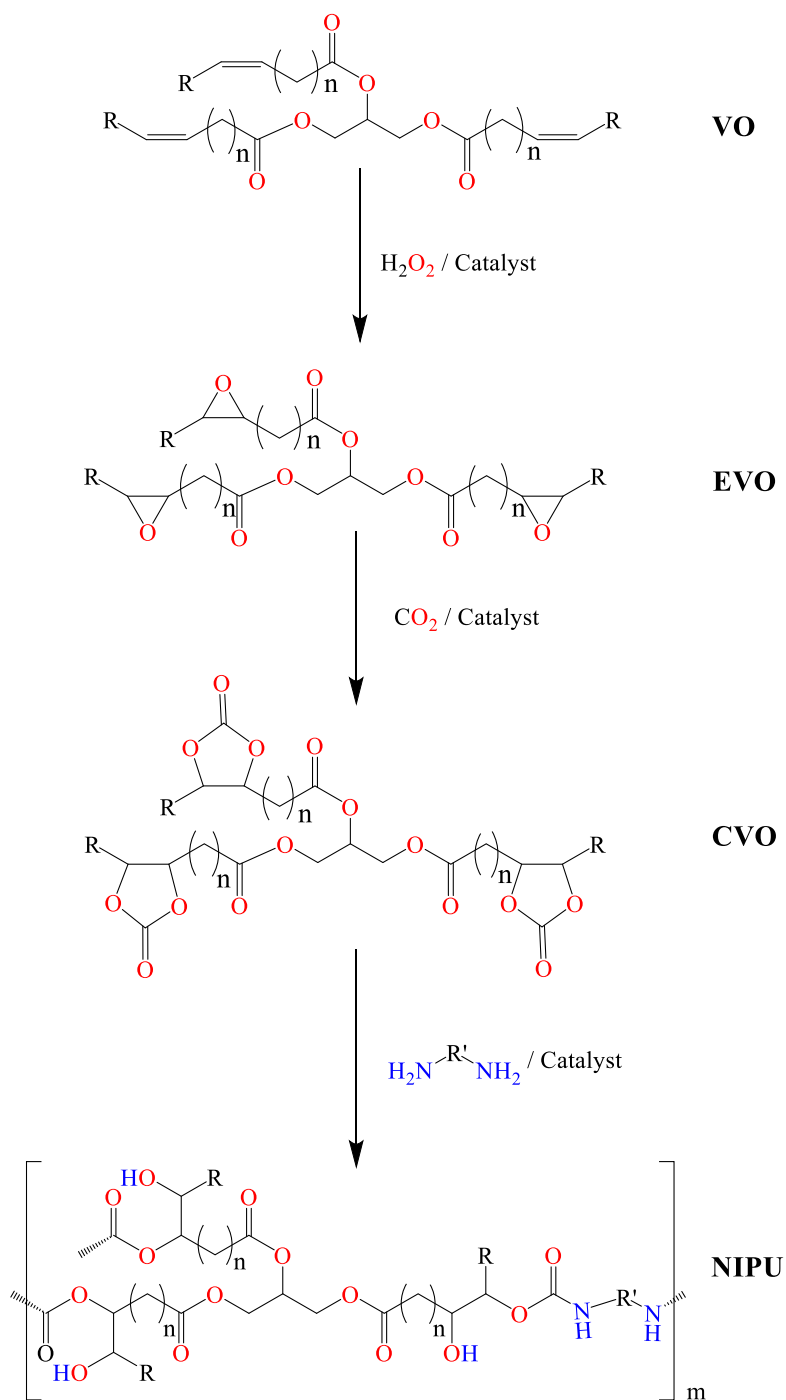
Figure 5. Reaction pathway for the synthesis of non-isocyanates polyurethanes (NIPUs) from vegetable oils.

1.5 Aim and scope of the research

The present scientific work focus on the further development of the reaction pathway for the production of non-isocyanate polyurethanes from a greener and safer point of view by application of catalysis, thermal analysis as well as mechanistic and kinetic investigations.

In the first step, the reaction pathway for the formation of polyurethane illustrated in Figure 5 was studied by using a model system. This strategy allows an easier quantification of the products and a better understanding of the mechanism and the kinetics. The methyl ester of oleic acid was used as a model compound of vegetable oils. Carbonated methyl oleate was obtained by means of epoxidation and carbonation reaction of the initially unsaturated methyl ester. Thereafter, the aminolysis of the carbonated methyl oleate was investigated.

The steric hindrance in the aminolysis process was explored. In this sense, the utilization of various amines in the aminolysis reaction can help to reveal the reactional behavior of the system as the lengths of the reactants are varied. Structure and reactivity relationships were evaluated.

Thermal risk assessment of the reactional pathway was also within the goals of this research study, for such, calorimetric analysis of the most exothermic reactions (i.e. epoxidation) was carried out in order to be able to propose suitable process alternatives to minimize the possibility of thermal runway scenarios. In this regard, adiabatic and isothermal calorimeters are efficient tool to precisely assess thermal risks. Various systems were compared and the epoxidation method with the lower risk of thermal runway was identified.

Potential heterogeneous catalysts for the different reaction steps including the carbonation reaction were investigated. The most important features were identified and their influence to the reaction advancement were established.
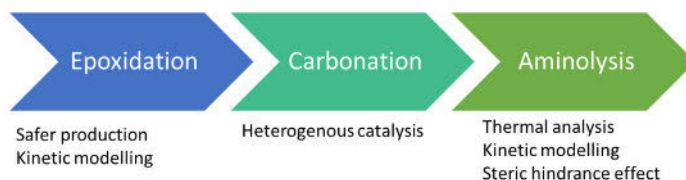

Figure 6. Research strategy.

2. Experimental section

2.1 Chemicals and materials

In the majority of the experimental studies the model substrates were derived from oleic acid (Sigma Aldrich, ≥90%). However, linseed oil (MP Biomedical, neat) and tall oils fatty acid TOFA (Forchem, neat) derivatives were used in some cases. Aqueous hydrogen peroxide solution (30-33 wt %) was provided by Fisher Scientific. Carbon dioxide was supplied by Linde plc and the amines used in the aminolysis reactions were provided by Alfa Aesar. Ethyl acetate solvent (≥99.9%) was obtained from Sigma Aldrich. Other chemicals used in the analytics were Hanus solution (0.1M), sodium thiosulfate solution (0.1M), cerium sulfate solution (0.1M), perchloric acid solution (0.1M), HCl solution (0.1M), tetraethylammonium bromide (≥98%), acetic acid (≥99%) and chloroform, (≥99.5%), all purchased from Sigma Aldrich . Ethanol (ETAX Aa) was obtained from ALTIA Industrial Oy.

The solid catalyst for the epoxidation reaction was obtained from LaRoche chemicals, a high performance Versal GH alumina with purity (≥96.7%) and only traces of other metal oxides such as SiO_2 and Fe_2O_3. The catalytic materials for the carbonation reaction, were prepared by means of propyl linking using silica-based materials as supports. Silica gel was provided by Merck & Co. and highly ordered silica SBA-15 was synthetized via a very well-known procedure [13] using tetraethyl orthosilicate (Sigma Aldrich , ≥ 98%) and triblock copolymer p123. The catalytic species were triethylamine (Fisher Scientific, ≥99%), tributylamine (Sigma Aldrich, ≥ 99%), 4-pyrrolidinopyridine (Sigma Aldrich, ≥98%) and Imidazole (Fisher Scientific, ≥99%)

2.2 Catalyst characterization techniques

2.2.1   Nitrogen physisorption

The textural properties of the catalytic materials were investigated by nitrogen physisorption using a Micrometrics 3Flex-3500 device. All samples were outgassed at 150 °C for 4 h prior to the measurement. Specific surface areas were calculated using the BET method. Other important textural features such as pore size distribution, total pore volume, microporous volume and mesoporous volume were determined too.

2.2.2   Fourier transmission infrared spectroscopy (FTIR)

The Brønsted and Lewis acid sites of the supports were determined with Fourier-transform infrared spectroscopy (FTIR) using pyridine (≥99.9%) as the probe molecule. Prior to measurement, the materials were shaped into small disks. The concentrations of acid sites were calculated from the recorded spectra in an ATI Mattson FTIR Infinity Series device.

2.2.3   Thermogravimetric analysis (TGA)

Thermogravimetric analysis of the synthetized materials was performed in a Mettler Toledo TGA/SDTA 851e instrument in order to estimate the amount of catalytic species attached to the surface of silica. The thermal decomposition temperature of the materials was also measured.

2.2.4   Transmission resolution electron microscopy (HR-TEM)

The surface structure of the supports and functionalized support were observed using high resolution transmission electron microscopy technique. The electron microphotographs were recorded in a JEM 1400 plus transmission electron microscope.

2.2.5   Induced plasma-optical emission spectroscopy (ICP-OES)

The rate between metal concentration and halide concentration on the catalytic materials were measured for both, fresh and spent catalyst with ICP optical emission spectroscopy in a Ciros CDD spectro analytical instrument.

2.3 Reactor systems

2.3.1   Double-jacked glass reactor

The epoxidation and aminolysis experiments were carried out using double-jacked glass reactor systems equipped with mechanical stirring, a thermostat and a condenser. The reaction temperature was measured with a sensor placed inside of the reactor vessel and the evolution of the temperature was recorded with an acquisition system connected to a computer. A more detailed description of the system is found in Figure 7. Batch and semi-batch modes of operation were explored for both, the epoxidation and the aminolysis reactions.
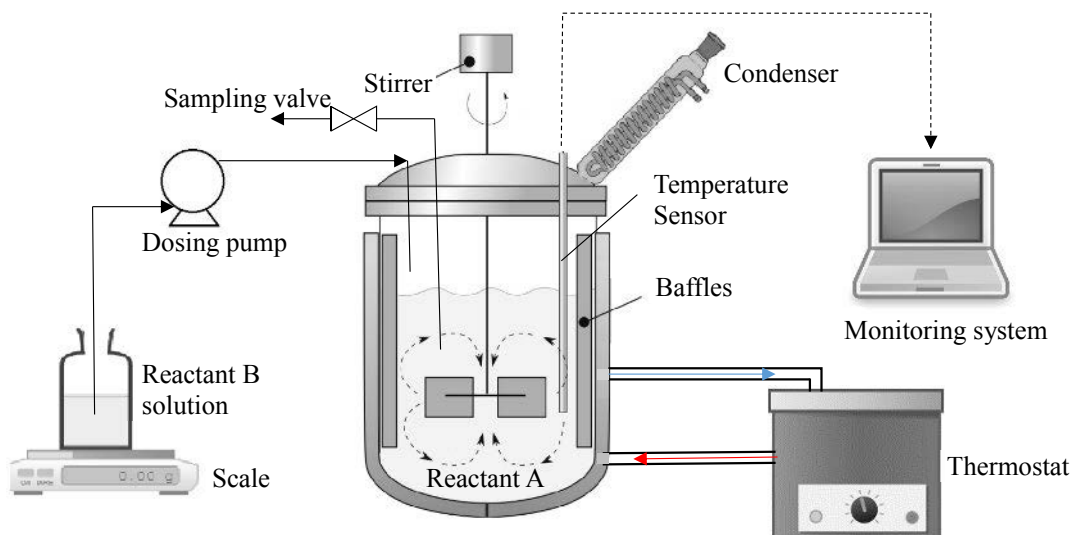
Figure 7. Schematic picture of the laboratory-scale glass reactor used in the epoxidation and aminolysis experiments.

2.3.2 Autoclave reactor

The carbonation experiments were conducted in a 300ml semi-batch Parr autoclave reactor equipped with mechanical stirring and electrical heating, where carbon dioxide was introduced to the system at a constant pressure of 30 bar during the total reaction time. The reactor system is displayed in Figure 8. All the experiments were conducted under isothermal conditions. Good mixing of the CO_2 and the slurry mixture of catalyst and epoxidized vegetable oil was ensured with a gas-entrainment impeller and vigorous stirring.

In a typical experiment, a determined amount of epoxidized vegetable oil and catalysts were mixed together in the autoclave vessel. Thereafter the reactor was sealed and air was purged out by flowing CO_2 three times. Then the reactor was heated to a target temperature and the reaction started by applying the desired CO_2 pressure to the system.
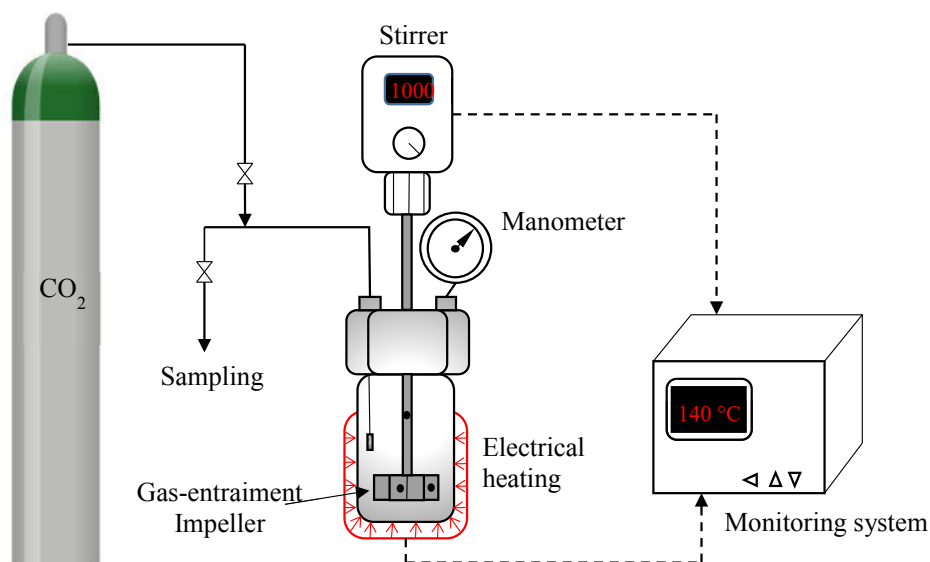
Figure 8. Schematic picture of the autoclave reactor used in the carbonation experiments.

2.4 Reaction calorimetry

2.4.1 Adiabatic calorimeter

The exothermicity of the various epoxidation system were investigated and compared using a pseudo-adiabatic calorimeter. The Advanced Reactive System Screening Tool (ARSST) is a calorimeter that can reach close-to-adiabatic conditions through the compensation principle by precisely following the temperature and proportionally adjusting the electrical heating. In brief, the system consists of a 10-mL glass test-cell, a heating belt and a magnetic stirrer. The test-cell is contained in a stainless steel autoclave vessel equipped with thermocouples and a pressure transducer. A more detailed description of the equipment is provided in Figure 9.

A mixture of vegetable, hydrogen peroxide and catalyst were introduced in the test-cell in a typical experiment. Thereafter the test-cell was housed in the autoclave containment vessel and a constant heating rate was applied. The system was kept under high nitrogen pressures in order to diminish evaporation. The reaction temperature was recorded until a runaway reaction was observed. The thermal risk assessment of the epoxidation systems was conducted by using safety criteria such as time-to-maximum rate under adiabatic condition (TMR$_{ad}$)
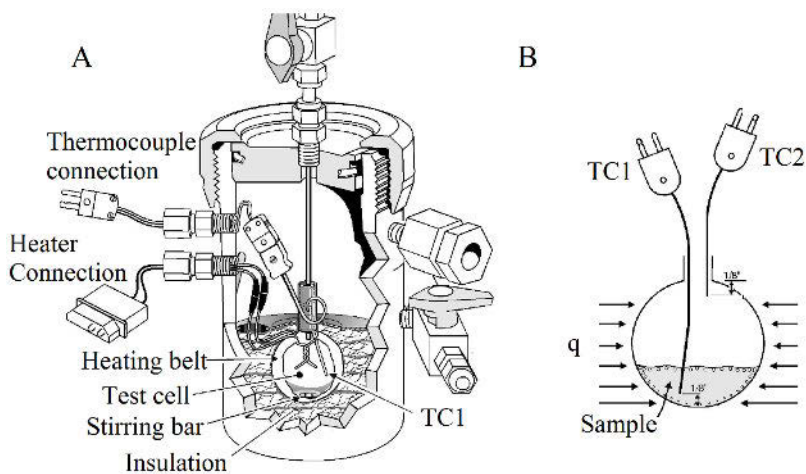
Figure 9. ARRST system schematics adopted from [14]: a) Containment vessel b) Test-cell.

2.4.2 Isothermal calorimeter

The reaction enthalpies of the aminolysis system were investigated using a Tian-Calvet calorimeter (C80 Setaram) under isothermal mode. A schematic view of the outside and internals of the calorimeter is displayed in Figure 10.

The target reaction reactants were placed in separated compartments in the measuring cell, on the other hand, the reference cell was filled with a non-reactive mixture of similar thermal properties to those of the measuring cell. Once the temperature and the heat flow rate were stabilized at the inside of the cells, the reaction was started by mixing the reactants in the measuring cell. The measured heat flow rate during the experiment is directly associated to the energy release due to the reaction and thus, reaction enthalpies. The enthalpies of the aminolysis reaction and the side reaction of amination were determined in this way.
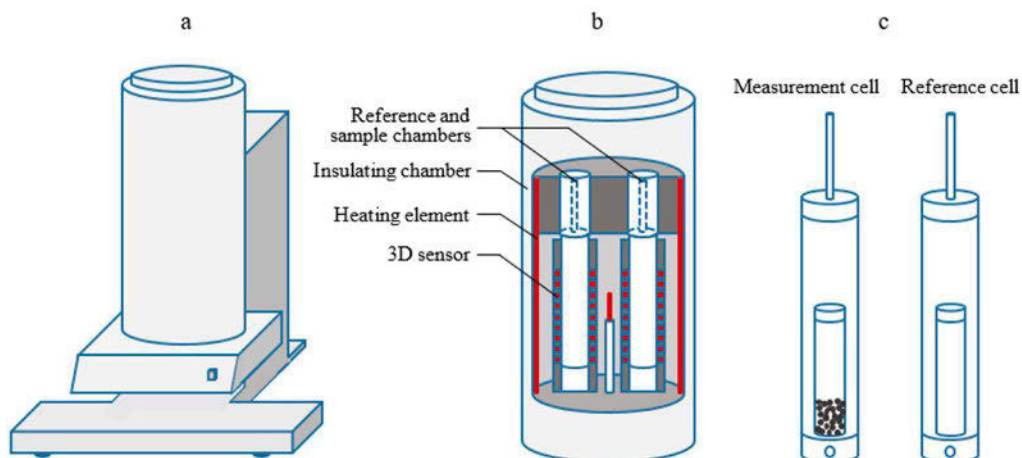
Figure 10. Schematic view of the C80 Seratam calorimeter adopted from [15]: a) outside view b) inside view c) reversal mixing cells.

2.5 Product analysis

2.5.1 Double bonds content

The reactant conversion during the epoxidation reaction step was calculated by quantification of the double bond content of the vegetable oil. Titration of the iodine value was performed using the Hanus method [16], in which samples were dissolved in chloroform, and the so-called Hanus solution consisting of iodine monobromide (0.1 M) in glacial acetic acid was added to halogenate the double bonds. The samples were then placed in the dark for 1 h. Thereafter a solution of potassium iodine (10% wt) in water was added along with 100ml of water followed by titration with a sodium thiosulfate standard solution (0.1N). The double bond content was calculated from the obtained iodine values.

2.5.2 Epoxide content

The epoxide (oxirane) content during the epoxidation and also the carbonation experiments was determined by using Jay's method [17]. The oils samples were first dissolved in chloroform followed by addition of a 20 wt% solution of tetraethylammonium bromide (TEAB) and finally titrated with a standard 0.1 M perchloric acid standard solution. An automatic potentiometric titrator (799 GPT Titrino, Metrohm) was used.

2.5.3   Hydrogen peroxide content

The inorganic phase hydrogen peroxide concentration during the epoxidation experiments was determined by the ceric sulfate titration method [18]. The samples were dispersed in a 5 wt% sulfuric acid solution. Ice blocks were added to the flask to maintain a temperature below 10 °C. Thereafter three drops of ferroin indicator were added to the samples followed by titration with a 0.1 N cerium sulfate standard solution until a clear-blue color was observed.

2.5.4   Carbonate content

The quantification of the cyclic carbonate during the carbonation and aminolysis reaction was carried out using FTIR technique. A calibration curve was obtained using carbonated vegetable oil and epoxidized vegetable oil mixtures of known concentrations. The FTIR spectra of carbonated vegetable oil has a strong band at 1804 cm^{-1} corresponding to the carbonated group, the absorbance of this peak was correlated to its concentration using the –CH group vibration at 2920 cm^{-1} as a reference band.

2.5.5   Physical properties

The dynamic viscosities of the oleic acid, methyl oleate and derivatives were measured with a VISCOBALL Viscometer (Fungilab.S.A., Spain) equipped with a Thermovisc series from Fungilab S.A. tempered at the range from 20℃ to 90℃.
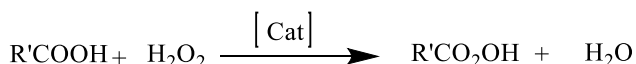
3. Epoxidation

3.1 Thermal risk assessment

The epoxidation step is presumably the most exothermic reaction in the reaction pathway for the production of non-isocyanate polyurethanes (NIPUs) from vegetable oils displayed in Figure 5. Hence, a detailed assessment of the thermal risk in the epoxidation system was conducted.
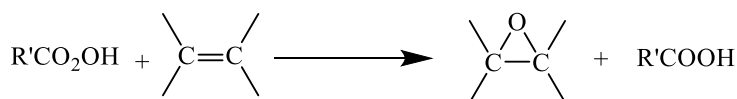
For the investigation of thermal risk associated to thermal explosion scenarios, which can take place during technical failures in which the generated heat cannot be efficiently removed, the best strategy is to recreate the event, i.e. in near adiabatic conditions. For this purpose the Advanced Reactive System Screening Tool (ARSST) calorimeter is ideal. The ARSST allows to reach the near adiabatic conditions of thermal runaway reactions at a minimalistic scale with no drawbacks and an accurate track of the pressure and temperature inside the test-cell.

a) Prileschajew epoxidation

    Aqueous phase:

$$R'COOH + H_2O_2 \xrightarrow{\left[Cat\right]} R'CO_2OH + H_2O$$

    Oil phase:

$$R'CO_2OH + \overset{\diagdown}{\underset{\diagup}{C}}{=}\overset{\diagup}{\underset{\diagdown}{C}} \longrightarrow \overset{\diagdown}{\underset{\diagup}{C}}\overset{O}{-}\overset{\diagup}{\underset{\diagdown}{C}} + R'COOH$$

- -

b) Direct epoxidation

$$H_2O_2 + \overset{\diagdown}{\underset{\diagup}{C}}{=}\overset{\diagup}{\underset{\diagdown}{C}} \xrightarrow{\left[Cat\right]} \overset{\diagdown}{\underset{\diagup}{C}}\overset{O}{-}\overset{\diagup}{\underset{\diagdown}{C}} + H_2O$$

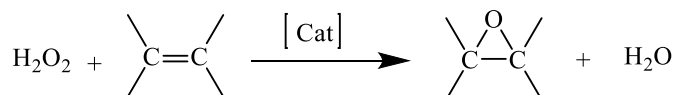Figure 11. Brief description of the studied epoxidation systems: a) Prileschajew epoxidation method, b) direct epoxidation method.

Two different epoxidation methods (displayed in Figure 11) were assessed and compared in terms of process safety, the Prileshcajew epoxidation method and the direct epoxidation method. The Prileschajew epoxidation system consists of an aqueous phase and an oil phase.

In the aqueous phase, the perhydrolysis of the oxygen carrier (a short-chain carboxylic acid) with hydrogen peroxide in the presence of homogenous or heterogeneous catalyst takes place, while the epoxidation of the double bond and regeneration of the oxygen carrier takes place in the oil phase. On the other hand, the direct epoxidation system consists only of hydrogen peroxide, the unsaturated vegetable oil and a solid catalyst (typically a metal oxide) in which the reaction takes places. Besides the main reaction (epoxidation), secondary ring-opening reactions of the epoxides are present in both systems.

Prileschajew epoxidation in the presence of formic acid and acetic acid

A determined amount of linseed oil (LSO) as the substrate, carboxylic acid, hydrogen peroxide and sulfuric acid as a catalyst was placed in the test cell. A constant heating rate (β) was applied ranging from 1 to 5 °C·min^{-1}. A nitrogen pressure of 34.4 bar was used in order to diminish the evaporation process. The initial temperatures of the experiment ranged from 20 to 35 °C. The influence of the carboxylic acid/double bond molar ratio, hydrogen peroxide/double bond molar ratio as well as the concentration of the homogenous catalyst were evaluated.

Direct epoxidation with hydrogen peroxide on an alumina catalyst.

A mixture of LSO, hydrogen peroxide and alumina as a heterogeneous catalyst were poured into the test cell. A constant heating rate in the range of 1-5 C·min^{-1} was applied. A nitrogen pressure of 34.4 bar was used in order to diminish the evaporation process. The initial temperatures of the experiment ranged from 20 to 35 °C.

3.1.1   Thermal risk

Different methods have been developed for the semi-quantification of the thermal risk associated to a chemical reaction [19]. Otherwise, the definition of the thermal risk is the combination of the severity and the probability of the occurrence. The adiabatic temperature rise (ΔT_{ad}) defines the severity and the time-to-maximum rate (TMR_{ad}) defines the probability of the occurrence to evaluate the thermal risk associated with a particular chemical system or chemical process (Figure 12).
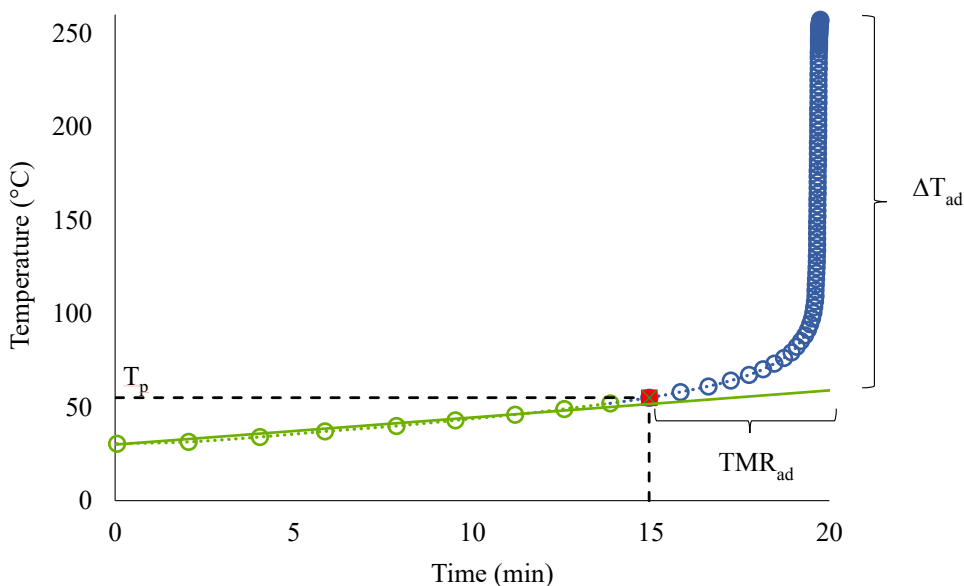
Figure 12. Typical temperature profile obtained from ARSST.

Adiabatic temperature rise (ΔT_{ad})

The potential of destruction of a chemical reaction is directly linked to its energy release. In a near adiabatic conditions system, where efficient cooling is not available, the temperature rise is proportional to the energy release. Therefore, the temperature is a convenient parameter to assess the severity. In contrast to chemical analysis, it is very easy to measure the temperature very accurately, which is a great benefit in thermal risk assessment. In Figure 12, it is clear that ΔT_{ad} can be obtained directly from the experimental data as the difference between the process temperature and the final temperature. Otherwise, ΔT_{ad} was not used in our work because it was found that the maximum temperature in most of the experiments were pretty much the same and thus displaying similar ΔT_{ad} values. The reason for this behavior is observed in Table 1. The maximum temperature was limited by the evaporation of the reaction mixture, which was very close to the boiling point of water (the majority component). Hence, this thermal risk parameter is not reliable under the operation conditions.

Table 1. Boiling temperature of water [20] and maximum temperature of the reaction mixture at different pressures.

Initial Pressure (bar)	Boiling point of water (°C)	Maximum temperature of the reaction mixture (°C)
7.51	170	177
21.37	198	217
34.40	243	243

Time to maximum rate (TMR$_{ad}$)

The time to maximum rate under adiabatic conditions (TMR$_{ad}$) at an initial process temperature (T_p) is defined as the elapsed time between the initial temperature and the maximum of the derivative (dT_p/dt) under adiabatic conditions. The estimation of this value for the epoxidation reaction at a particular process temperature (T_p) can be easily obtained from the experimental data as illustrated in Figure 12.

For a zero-order reaction, TMR$_{ad}$ is defined by the expression:

$$\mathrm{TMR}_{ad}\left(T_P\right) = \frac{m_{\mathrm{R}} \cdot \hat{\mathrm{C}}_{\mathrm{PR}} \cdot \mathrm{R} \cdot T_P^2}{E_a \cdot \mathrm{q}_{\mathrm{R}}\left(T_P\right)} \tag{1}$$

where T_P is the process temperature, i.e., initial temperature, m_{R} is the reaction mass, $\hat{\mathrm{C}}_{\mathrm{PR}}$ the specific heat capacity of the reaction mixture, R is the general gas constant, E_a is the activation energy and $q_R(T_P)$ is the heat release rate due to chemical reactions at the process temperature.

The utilization of this expression of zero-order kinetics is a very conservative approach, in which a worst case is considered because the reaction rate does not slow down during the progress of reaction, as the 1st, 2nd and higher order kinetics. Smaller values of TMR$_{ad}$ are obtained in the zero order kinetics approach.

3.1.2 Thermal risk comparison

In order to rank the three different epoxidation methods from a risk point of view, the TMR_{ad} was used as a reliable parameter. The probability of the occurrence of a runaway reaction, in the epoxidation process by Prileschajew method and by the direct epoxidation were evaluated and compared using a semi-quantitative six level scale [19] (reported in Table 2). The probability is considered high if the TMR_{ad} values are superior to 8 h (1 working shift). However, it is worth noting that this scale is only an order of magnitude approach and that at an industrial level, the probability depends on many other factors related to the working environment such as the reactor size, the degree automation, training of the personal and so on.

Table 2. Assessment criteria for TMR_{ad}.

Simplified	Extended	TMR_{ad} (h)
High	Frequent	< 1
	Probable	4-8
Medium	Occasional	8-24
Low	Seldom	24-50
	Remote	50-100
	Almost Impossible	>100

The concentration of formic acid was found to have a strong influence on the probability of the occurrence of a runaway event for the Prileschajew epoxidation technology from 40 °C to 80 °C, which is a typical operation range for this system. For most of the screened molar ratios, the probability of occurrence was high, ranging between probable and frequent (Table 3a). In the case of hydrogen peroxide molar ratios (Displayed in Table 3b), a similar tendency was observed. Higher concentrations of these two components resulted in shorter TMR_{ad} values. On the other hand, if sulfuric acid was used as the catalyst, no important changes in the TMR_{ad} were observed. The possible reason for this behavior might be related to the autocatalytic effect already provided by the formic acid, which makes the kinetics of this system very rapid compared to other carboxylic acid epoxidation systems, such as the one of acetic acid. In general, the probability of a runaway reaction for the Prileschajew epoxidation by formic acid was found to be extremely high. Very rapid kinetics and high exothermicity of this system makes it difficult to keep a good control of the operation conditions, and thus small deviations could lead to profound temperature rises and undesired ring-opening reactions as a secondary process. This is one of the main reasons why the research interest in the recent years has been focused towards the use of acetic acid instead.

Table 3. Probability of thermal runaway for the Prileschajew epoxidation in the presence of formic acid.

a)

T_p (°C)	DB: FA molar ratio			
	1:0.5	1:1	1:1.3	1:1.6
20	probable	probable	probable	frequent
30	probable	frequent	frequent	frequent
40	probable	frequent	frequent	frequent
50	frequent	frequent	frequent	frequent
60	frequent	frequent	frequent	frequent
70	frequent	frequent	frequent	frequent
80	frequent	frequent	frequent	frequent

b)

T_p (°C)	DB:HP molar ratio		
	1:1	1:1.4	1:1.8
20	probable	frequent	frequent
30	frequent	frequent	frequent
40	frequent	frequent	frequent
50	frequent	frequent	frequent
60	frequent	frequent	frequent
70	frequent	frequent	frequent
80	frequent	frequent	frequent

c)

T_p (°C)	Sulfuric acid loading			
	0 wt%	1 wt%	2 wt%	3 wt%
20	probable	probable	probable	probable
30	frequent	frequent	frequent	frequent
40	frequent	frequent	frequent	frequent
50	frequent	frequent	frequent	frequent
60	frequent	frequent	frequent	frequent
70	frequent	frequent	frequent	frequent
80	frequent	frequent	frequent	frequent

The probability of the occurrence of a runaway scenario for the epoxidation in the presence of acetic acid is displayed in Table 4 and as it can be noticed, the concentration of acetic acid has an important effect on TMR_{ad}. At low temperatures and concentrations of acetic acid, the system is in low probability zone. Otherwise, if high temperature and concentration of acetic acid are used the system leans towards frequent occurrence of runaway. The hydrogen peroxide

concentration was found to have a small impact on TMRad at temperatures below 60° C, but at temperatures exceeding 60°C the probability is frequent.

Table 4. Probability of thermal runaway for the Prileschajew epoxidation in the presence of acetic acid.

a)

T_p (°C)	DB:AA molar ratio			
	1:0.5	1:1	1:1.4	1:1.8
20	Impossible	occasional	occasional	occasional
30	remote	probable	probable	probable
40	seldom	probable	probable	probable
50	occasional	probable	probable	probable
60	probable	probable	probable	probable
70	probable	probable	frequent	frequent
80	probable	frequent	frequent	frequent

b)

T_p (°C)	DB:HP molar ratio	
	1:1.4	1:1.8
20	occasional	occasional
30	probable	probable
40	probable	probable
50	probable	probable
60	probable	probable
70	frequent	frequent
80	frequent	frequent

c)

T_p (°C)	Sulfuric acid loading			
	0 wt%	1 wt%	2 wt%	3 wt%
20	occasional	occasional	probable	probable
30	probable	probable	probable	frequent
40	probable	probable	probable	frequent
50	probable	probable	frequent	frequent
60	probable	frequent	frequent	frequent
70	frequent	frequent	frequent	frequent
80	frequent	frequent	frequent	frequent

Epoxidation in the presence of acetic acid is normally performed in the presence of catalysts in order to achieve high epoxide yields. The catalysts for the perhydrolysis step are mainly mineral acids and ion-exchange resins, among those sulfuric acid is a very typical one. It is notable from Table 4c, that addition of sulfuric acid catalyst increases considerably the probability of thermal

explosion in the system. Overall, the runaway scenario of the Prileschajew epoxidation in the presence of acetic acid can be categorized as probable/frequent at 50°C to 70 °C, which is a typical operation temperature range for this system.

Table 5. Probability of thermal runaway for the direct epoxidation using H_2O_2 on an alumina catalyst.

A)

Tp (°C)	Catalyst loading			
	0 wt%	10 wt%	20 wt%	30 wt%
20	impossible	impossible	impossible	seldom
30	impossible	remote	seldom	occasional
40	impossible	seldom	occasional	occasional
50	remote	occasional	occasional	probable
60	seldom	probable	probable	probable
70	occasional	probable	probable	probable
80	probable	probable	probable	probable

B)

Tp (°C)	DB:HP molar ratio		
	1:1	1:2	1:3
20	impossible	seldom	occasional
30	impossible	seldom	occasional
40	remote	occasional	probable
50	seldom	probable	probable
60	occasional	probable	probable
70	probable	probable	probable
80	probable	probable	frequent

In the direct epoxidation on alumina catalyst, Table 5 shows mainly low probabilities of a runaway event. At temperatures lower than 50° C, the probability of runaway is mostly low. Higher process temperatures lead to medium probabilities of the occurrence, except if high concentration of hydrogen peroxide are used, as shown in Table 5B. However, the normal operation conditions of this system range between 70-80 °C with catalyst loadings below 10 wt%, from Table 5 it can be concluded that the general probability of thermal runaway is probable with a very slight inclination to frequent.

If the treated epoxidation systems are compared from the view point of thermal safety using the probability of the occurrence of a thermal runaway reported in this work as the safety criterion, the direct epoxidation on alumina is the one with the lower values of TMR_{ad}, followed by Prileschajew epoxidation in the present of acetic acid, and lastly in the presence of formic acid.

3.2 Reaction kinetics

The kinetics of the direct epoxidation of methyl oleate as a model substrate with hydrogen peroxide and alumina as the catalyst was investigated.

3.2.1   Catalyst characteristics

Versal GH (LaRoche Chemicals) was utilized as the epoxidation catalyst, which is a high-performance catalytic grade gamma alumina. This γ-alumina has been used by our group in a previous work [21]. Therefore, the catalyst characteristics are briefly summarized from the previous research and as well as from data provided by the catalyst manufacturer in Table 6.

Table 6. Principal characteristics of the catalyst.

	Chemical Analysis (wt %)							Physical properties			
	Na_2O	Fe_2O_2	SiO_2	SO_4	Cl	Al_2O_3	LOI*	Loose bulk density $(g \cdot mL^{-1})$	Surface area $(m^2 \cdot g^{-1})$	Acid dispersibility (%)	Phase
Versal GH	0.07	0.04	0.1	0.03	0.1	96.7-98.7	1-3	0.59	270	<10	Gamma

* Loss on ignition

3.2.2   Selection of the reactor mode: batch or semi-batch?

A mixture of methyl oleate, the catalyst and ethyl acetate as the solvent was poured into a 500 mL glass reactor equipped with mechanical agitation by a Rushton turbine impeller, baffles and a reflux condenser (Figure 7). At the first stage, some experiments were conducted using a batch reactor set-up to reveal the qualitative behavior of the system. It was found that the double bond conversion and epoxide yield were relatively low, 60 % and 45% respectively. The explanation for this outcome lies on the hydrogen peroxide interaction with the catalyst (Figure 13). During the first experiments, it was observed that hydrogen peroxide was consumed rather rapidly and very little was destinated to the epoxidation process on the catalyst surface, which suggests that the catalytic decomposition of hydrogen peroxide into water and oxygen is dominant in the batch reactor system.
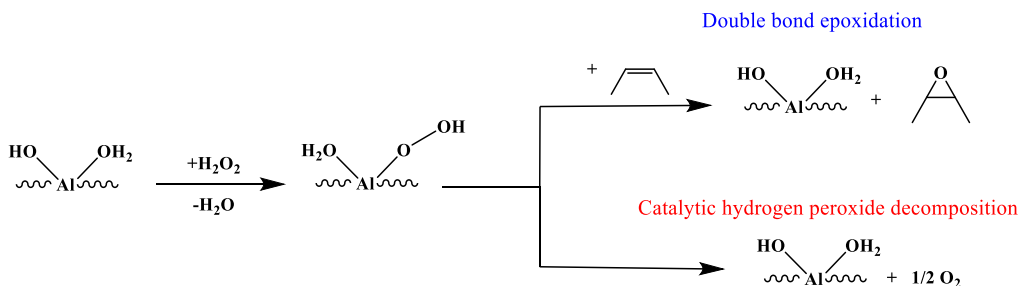
Figure 13. Simplified reaction scheme of the catalytic epoxidation and hydrogen peroxide decomposition on γ-alumina.

In a batch reactor setup, where a high concentration of hydrogen peroxide is present at the beginning, the decomposition rates can negatively reduce the available hydrogen peroxide, which forms the necessary active sites that later react with the double bonds of the vegetable oil to yield the epoxide. After four hours of reaction, around 50% of the total hydrogen peroxide was consumed under this experimental configuration (Figure 14). Conversely, as a semi-batch reactor set-up was adopted, the addition of fresh hydrogen peroxide at a constant dosing rate helped to maintain an increasing concentration of hydrogen peroxide in the reactor until the addition was stopped. Thereafter, the hydrogen peroxide concentration behaved similarly to that of the batch experiments. Figure 14 confirms that when the same amount of hydrogen peroxide is gradually loaded into the reactor at low dosing rates over an extended period, a better reaction environment with a higher hydrogen peroxide concentration is maintained.
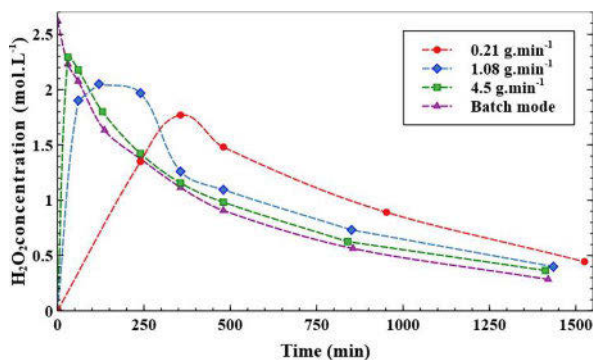

Figure 14. Hydrogen peroxide concentration evolution under batch and semi-batch conditions at 74 °C, DB: HP = 1:4 and 10 wt% of γ-alumina catalyst.

Figure 15 demonstrates clearly that the operation under semi-batch conditions significantly improves the reactant conversion and the product yield in the epoxidation reaction: an

improvement of more than 30% was observed when low-flow semi-batch conditions were applied compared to batch operation under identical conditions.
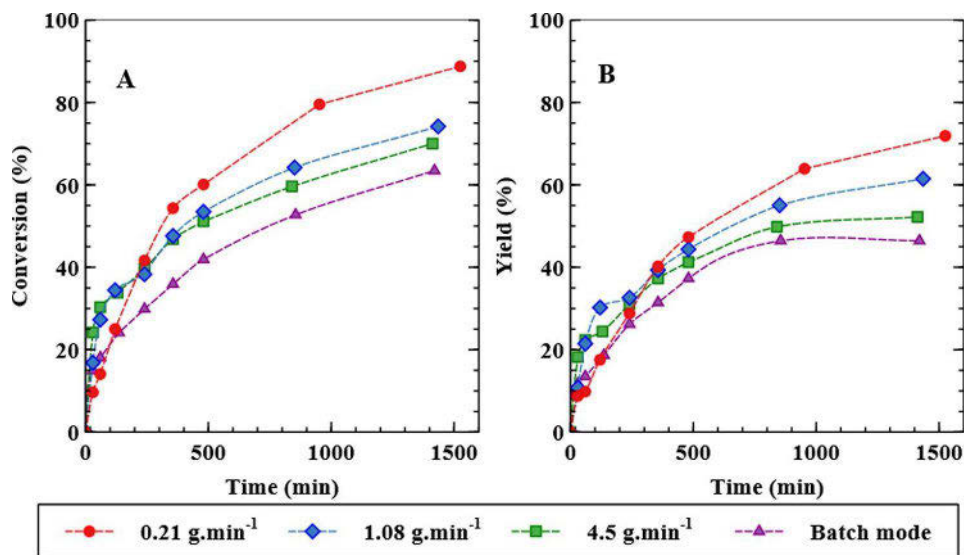

Figure 15. Epoxidation under batch and semi-batch conditions at 74 °C, DB:HP = 1:4 and 10 wt% catalyst; (a) Double bond conversion, (b) Epoxide yield.

3.2.3 External and internal mass transfer resistance

Because this system is a complex liquid-liquid-solid reaction, involving the utilization of bulky substrates with restrictive diffusion capability and limited reactivity, it was pertinent to determine whether or not mass transfer resistances influenced the observed reaction rates. The limitations to operate within an intrinsic kinetic regime were checked following a classical but reliable tests routines based on the quantification of the productivity as the function of the catalyst particle size and the stirring speed.

Experiments at different stirring velocities but keeping the other parameters on fixed levels were systematically conducted to evaluate the interfacial mass transfer resistances of the species. The concentration of the primary reaction product (oxirane) was utilized as the measure of the productivity. Samples were analyzed at different reaction times. From Figure 16a, it can be deduced that the operation with stirring velocities exceeding 500 rpm evidently ensures enough of liquid-phase turbulence in the system to suppress the external mass transfer limitations around the catalyst particle. The more or less constant product concentration at

different stirring velocities is a clear indication that the system operated in a kinetic regime at stirring speed exceeding 500 rpm.
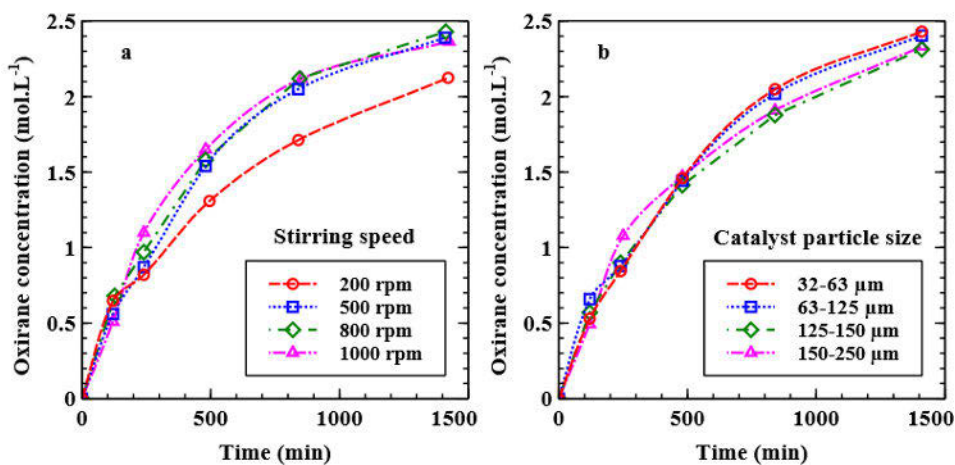

Figure 16. Mass transfer resistance evaluation; (a) External mass transfer verification at 74 °C, DB:HP = 1:4, 0.22 g·min^{-1} and 10 wt%. (b) Internal mass transfer verification at 74 °C, 800 rpm, DB:HP = 1:6, 0.22 g·min^{-1} and 5 wt% catalyst.

The influence of internal mass transfer, i.e., the diffusion inside the catalyst pores, was checked. The dependence of the catalytic activity on the particle size was verified by measuring the productivity, i.e. the kinetics of oxirane formation for different catalyst particle diameters. The catalyst material used in the experiments was sieved to obtain fractions with different particle diameters. The results are displayed in Figure 16b.

The progress of the oxirane concentration as a function of the reaction time was very similar for the different catalyst particle sizes. Because the catalyst mainly consisted of very fine particles (<250 micrometers), the operation within the regime of intrinsic kinetics was confirmed and no internal diffusion limitations whatsoever were observed.

In conclusion, no mass transfer limitations of any kind were evidenced in the experiments. Therefore, these phenomena were excluded from the mathematical modelling, which was based only on the intrinsic kinetics.
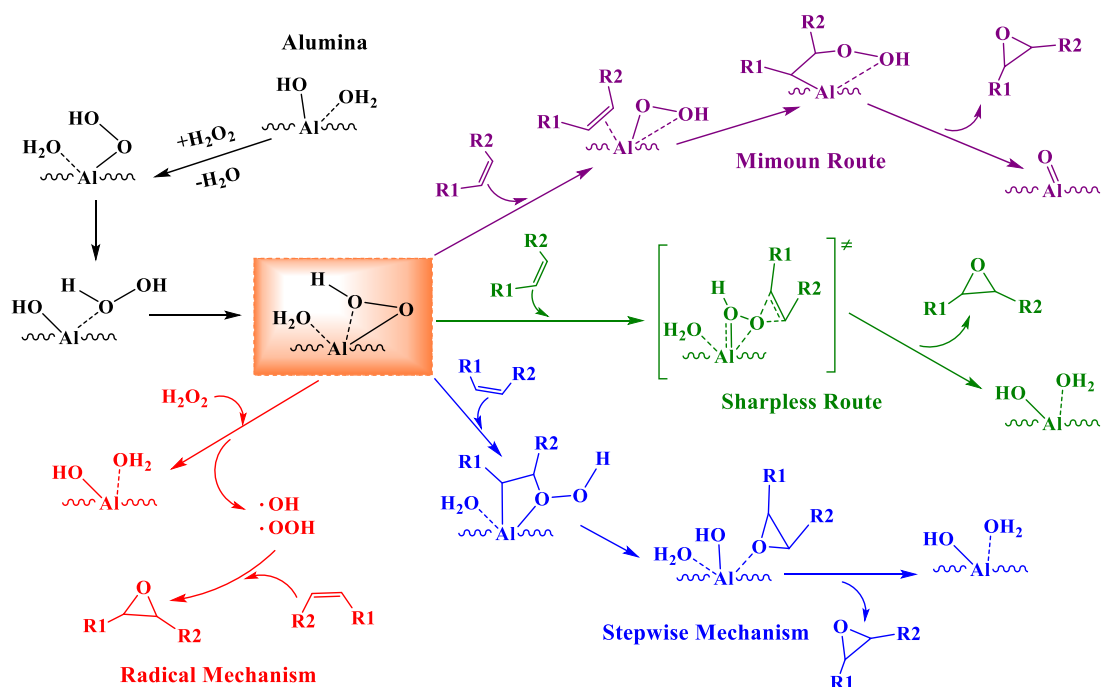
3.2.4 Kinetic modelling of epoxidation

Figure 17. Plausible reaction mechanisms for the olefin epoxidation in the presence of an alumina catalyst.

Diverse reaction pathways have recently been proposed for the olefin epoxidation on alumina catalyst. The possible reaction routes derived from density functional theory (DFT) studies [22] are displayed in Figure 17. From the viewpoint of fundamental chemical thinking, the rival mechanisms are quite different, but they have a common feature: the formation of a hydroperoxyl adduct on the alumina surface. Thus, a common step for the reaction sequence is presumed to be the activation of the OH ligands on the alumina surface through reaction with hydrogen peroxide, leading to the formation of a hydroperoxyl group and release of water from the catalyst surface. The hydroperoxyl group is then able to further react with the double bond of the methyl oleate and after several intermediate steps, the epoxide group is finally formed, thereafter the epoxidized product is desorbed from the catalyst surface.

The stepwise mechanism and the Sharpless route are very similar. In fact, these are the most viable routes for the reaction to develop, according to literature [23] these pathways present the lowest energy barrier. Both reaction paths can be compressed to a four-step mechanism. Firstly, the hydrogen peroxide reacts with the OH groups on the alumina catalyst surface to form a

hydroperoxyl adduct, then the double bonds of the vegetable oils reacts with the hydroperoxyl species on the alumina surface to produce an intermediate specie, which eventually afford the oxirane product and regenerate the catalyst. The parallel process of the hydroperoxyl species decomposition into oxygen and former OH is also included. The compressed mechanism is displayed below.

	ν_1	ν_2	
HP + OH* = OOH* + W	1	1	(I)
OOH* → OH* + (1/2)O_2	0	1	(II)
OOH* + DB → I*	1	0	(III)
I* → EP + OH*	1	0	(IV)
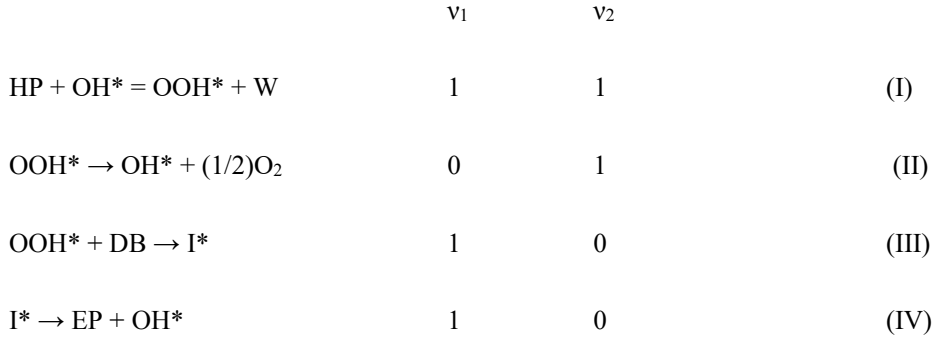
Note: *(*II) is a simplified form of the real surface mechanism, probably proceeding stepwise

In the above reaction scheme, HP is hydrogen peroxide, OH is the hydroxyl group, OOH is the hydroperoxyl adduct, W is water, DB is the organic component with a double bond (e.g. fatty acid or fatty acid ester), EP is the epoxidized product, * is a vacant site and I is the reaction intermediate.

The stoichiometric numbers ν_1 and ν_2 reflect the steps participating in the epoxidation and hydrogen peroxide decomposition routes. The sum of steps 1, 3 and 4 gives

DB+ HP → EP + W   double bond epoxidation Route I

while the sum of steps 1 and 2 gives

HP → W + 1/2O_2 hydrogen peroxide decomposition Route II
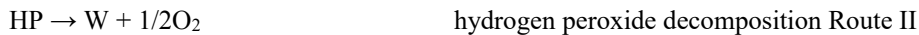
From the previously proposed four-step mechanism and in a standard manner by assuming quasi-steady states for all the adsorbed species, the rate equations for the epoxidation process and the hydrogen peroxide decomposition on the surface of alumina are obtained,

$$r_I = \frac{k_I c_{DB} c_{HP}}{1 + \alpha c_{DB} + \beta c_{HP} + \gamma c_{DB} c_{HP} + \omega c_W} \tag{2}$$

$$r_{II} = \frac{k_{II}c_{HP}}{1 + \alpha c_{DB} + \beta c_{HP} + \gamma c_{DB}c_{HP} + \omega c_W} \tag{3}$$

where k_I, k_{II}, α, β, γ and ω are merged rate parameters, while r_I and r_{II} denote the catalytic epoxidation and hydrogen peroxide decomposition rates, respectively. The operative parameters to be estimated by nonlinear regression analysis using experimental data are k_I, k_{II}, β, γ and ω with their respective activation energies.

Non-catalytic reactions

For the non-catalytic reactions (r'_i), i.e. the decomposition of hydrogen peroxide and the non-catalytic epoxidation simple semi-empirical kinetic expressions were applied.

The following power-law expression was used for the hydrogen peroxide decomposition,

$$r'_{II} = k'_{II} \cdot c_{HP}{}^{\lambda} \tag{4}$$

The value of the exponent (λ) was adjusted in order to get the best possible fit to the experimental data describing the concentration of hydrogen peroxide.

It was also observed that non-catalytic epoxidation takes place in the system at a minor extent. Hence, some independent experiments in the absence of alumina catalyst were carried out to obtain an acceptable approximation of this reaction rate. The kinetics of this process was described as follows,

$$r'_I = k'_I \, c_{HP}c_{DB} \tag{5}$$

The influence of ring-opening reaction was confirmed to be low in the experiments. The kinetics of ring-opening was described with the simple formula

$$r'_{RO} = k'_{RO} \, c_{EP} \tag{6}$$

Component mass balance in the semi-batch reactor

The mass balance of each component in the system was expressed using the characteristic semi-batch reactor balance equation,

$$\frac{dc_i}{dt} = \frac{(c_{0i} - c_i)/\tau_0}{1 + t/\tau_0} + \frac{r_i \rho_{0B}}{1 + t/\tau_0} + r'_i \qquad (7)$$

Equation (7) describes the concentration evolution of an individual component (i) in the reactor. The terms r_i and r'_i denote the catalytic and non-catalytic generation rates of the components, respectively. The initial catalyst bulk density (ρ_{0B}) and the space time (τ_0) are described by the expressions, $\rho_{0B} = m_{cat}/V_{0L}$ and $\tau_0 = V_{0L}/V'$ respectively.

The liquid volumes were assumed to be additive, which implies that a simple update formula for the liquid volume (V_L) is applied,

$$V_L = V_{0L} + V't \qquad (8)$$

where V_{0L} is the initial volume and V' is the volumetric flow rate (the feed rate of the aqueous hydrogen peroxide solution).

Parameter estimation results

A differential equation system was obtained when the generation rates of each component were inserted in Equation (7), which describes the component mass balances. The initial concentrations of the components in the reactor were all known, and they were used as the initial conditions for the solution of the differential equation model. The correlation between the pre-exponential factors and the activation energies was suppressed by using a modified form of the Arrhenius equation,

$$k_i(T) = k_i(T_{ref}) \cdot \exp\left(\frac{-E_a}{R}\left(\frac{1}{T} - \frac{1}{T_{ref}}\right)\right) \qquad (9)$$

where k_i is reaction rate constant, E_a is the activation energy, R is the universal gas constant, T and T_R denote the reaction temperature and reference temperature, repectively.

The differential equation system of initial value problem was solved numerically with respect to the reaction time using a stiff ODE solver algorithm (ODESSA). One homogenous phase was assumed for the mass balances. The minimum of the error squares between experimentally recorded and predicted (equation 10) concentrations was searched with a combined simplex-

Levenberg-Marquardt algorithm. The software ModEst [24] was used to carry out the numerical operations. The objective function in the regression analysis was defined as follows,

$$OF = \sum (C_{i,\exp} - C_{i,sim})^2 \qquad (10)$$

where $C_{i,exp}$ is the experimental concentration and $C_{i,sim}$ is the concentration simulated by the mathematical model.

The reliability of the model to adjust to the experimental data was evaluated by the coefficient of determination,

$$R^2 = 1 - \frac{\sum (C_{i,\exp} - C_{i,sim})^2}{\sum (C_{i,\exp} - \overline{C}_{i,\exp})^2} \qquad (11)$$

where $\overline{C}_{i,\exp}$ is the average value of the experimental concentration.

During the course of the parameter estimation it was noticed that the merged parameters β and γ converged to very low values compared to the rest of the parameters. Thus, stripped versions of the rate expressions, equations 2 and 3 were used, only taking into account k_I, k_{II}, ω and the parameter and $\alpha = (k_I/k_{II})$. In this sense, the total number of parameters estimated by regression analysis was reduced to six.

A summary of the modeling results is displayed in Figure 18. A relatively good fit (>90%) was achieved with a rather good description of the experimental data within the model.
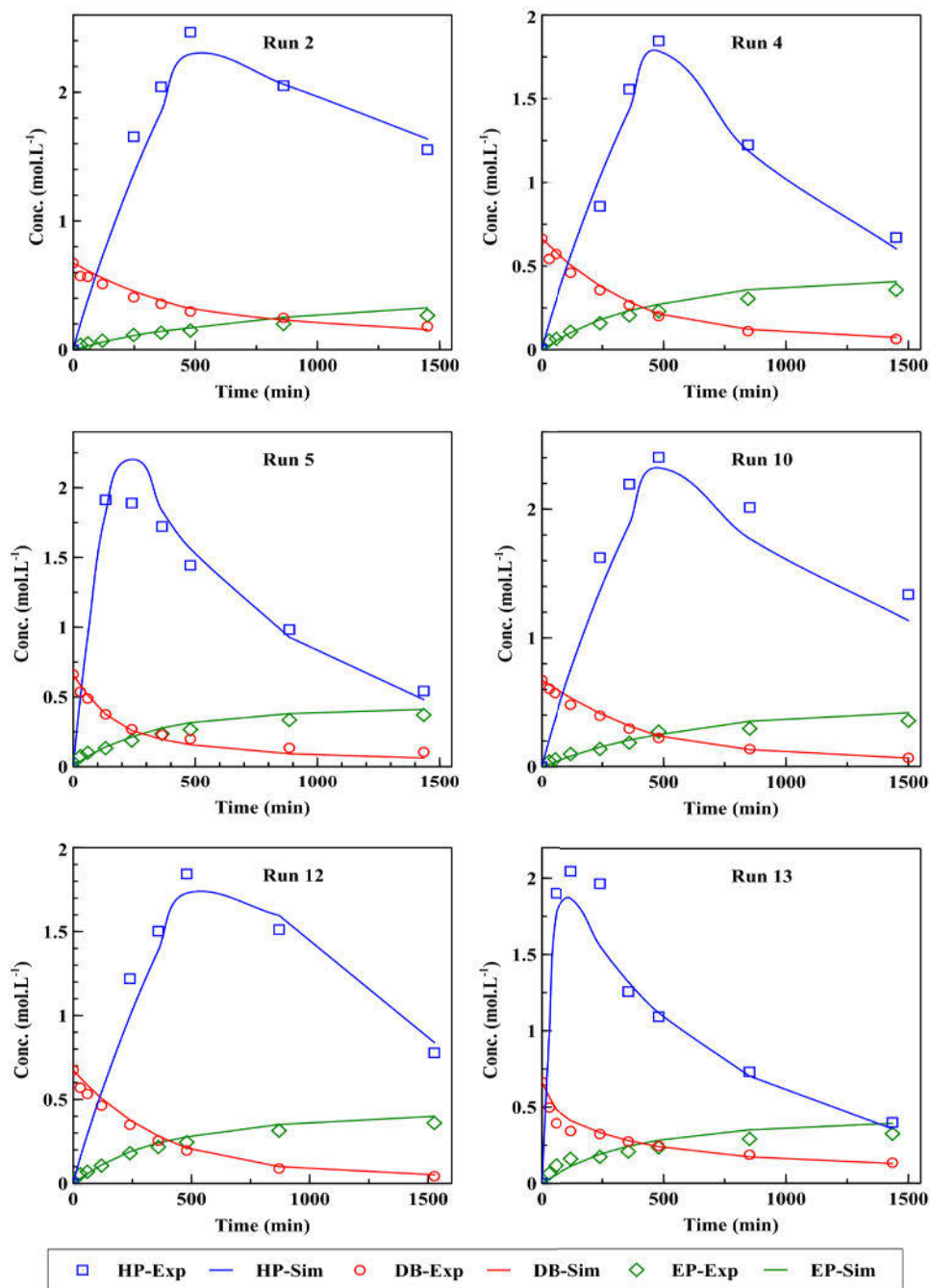
Figure 18. Fit of the mathematical model to the experimental data for the alumina-catalyzed epoxidation of methyl oleate as a model compound.

The standard deviations of the parameters were found to be at acceptable levels (Table 5). In the case of parameter ω, a relatively high deviation was observed, possibly because of the water concentration being simulated. A moderate correlation between the kinetic constants at the reference temperature and the activation energies was observed confirmed by the correlation matrix (Table 6). In conclusion, the model was proved to be capable of predicting the reaction evolution within a wide range of operational conditions.

Table 7. Parameter estimation results for catalytic epoxidation of methyl oleate at $T_{ref} = 70\ °C$.

	Estimated parameter	Estimated Std Error	Est. Relative Std Error (%)
k_I	4.97E-05	1.87E-05	37.6
k_{II}	6.53E-05	2.38E-05	36.4
ω	2.00E-01	1.26E-01	63.2
Ea_I	1.01E+05	3.56E+04	35.3
Ea_{II}	1.22E+05	2.14E+04	17.5
Ea_ω	1.06E+05	4.67E+04	44

Units: $k_I = (L^2 \cdot mol^{-1} \cdot g^{-1} \cdot min^{-1})$; $k_{II} = (L \cdot g^{-1} \cdot min^{-1})$; $\omega = (L \cdot mol^{-1})$; $Ea = (J \cdot mol^{-1})$

Table 8. Correlation matrix of the kinetic parameters.

	k_I	k_{II}	ω	Ea_I	Ea_{II}	Ea_ω
k_I	1.000					
k_{II}	0.825	1.000				
ω	0.823	0.970	1.000			
Ea_I	0.024	0.299	0.222	1.000		
Ea_{II}	0.483	0.490	0.378	0.351	1.000	
Ea_ω	-0.15	-0.203	-0.391	0.264	0.615	1.000

4. Carbonation

Carbonation of epoxidized vegetable oils (Figure 19) is predominantly carried out using ammonium halides salts and alkali metal halide salts as efficient homogenous catalysts. Otherwise, very little is available about single-component heterogeneous catalysts for the carbonation of epoxidized vegetable oils, most of the reported systems using heterogeneous catalysts are co-catalyzed ones, requiring of homogenous species in order to proceed [25]–[27].

The heterogeneous catalysis of the carbonation process was investigated. Four different nucleophilic catalysts were immobilized thought propyl linkages procedures into silica-based supports and screened as possible heterogeneous catalysts for the carbonation of epoxidized methyl oleate. The catalysts most important features and thier effects on the carbonation process were evaluated.
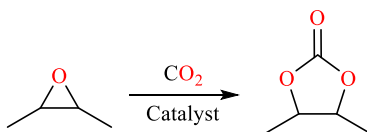

Figure 19. Simplified carbonation process.

4.1 Heterogeneous catalysis in the carbonation process

4.1.1   Catalyst preparation

The utilization of silica anchored nucleophiles as active species in the cycloaddition reaction of carbon dioxide to epoxidized vegetables oils was investigated using epoxidized methyl oleate (EMO) as the substrate. Triethylamine (TEA), tributylamine (TBA), imidazole (Imid) and 4-pyrrolidinopyridine (4PP) were supported onto silica-based materials. The influence of the catalyst pore size was explored by using silica gel and highly ordered mesoporous silica SBA-15 as supports. Moreover, the influence of a hydrogen bond donor (HBD) was also evaluated by doping the support with a Lewis metal centre.

A commercial silica gel support was calcined at 500 °C with a heating rate of 3 °C·min^{-1} for 12 hours before the use. Zn-SBA-15(x), (where x is the Zn/Si molar ratio) was prepared as it follows: 2.0 g of triblock copolymer (pluronic123) and a determined amount of zinc nitrate hexahydrated were dissolved in 75 mL HCl 1.6M for 4 h at 40 °C. After complete dissolution,

4.0 g of tetraethyl orthosilicate (TEOS) was added slowly. The solution was stirred and kept at 40 °C for 24 h. The resulting mixture was transferred to a Teflon liner and heated to 100 °C in an autoclave for another 24 h under static conditions. Thereafter, the mixture was filtrated and the white solid was calcined at 550°C with a heating rate of 1 °Cmin^{-1} for 6 h.

All supported catalytic materials were prepared via very well-known propyl linkage procedures with few modifications. The silica supports were first iodine functionalized by anchoring (3-iodopropyl)trimethoxysilane species onto the surface in a toluene reflux under inert gas atmosphere for 24h. Thereafter, the catalytic species were attached to the propyl linkage on the support surface in a toluene reflux and inert gas atmosphere with different synthesis time. A brief overview of the synthesis procedure is displayed in Figure 20.
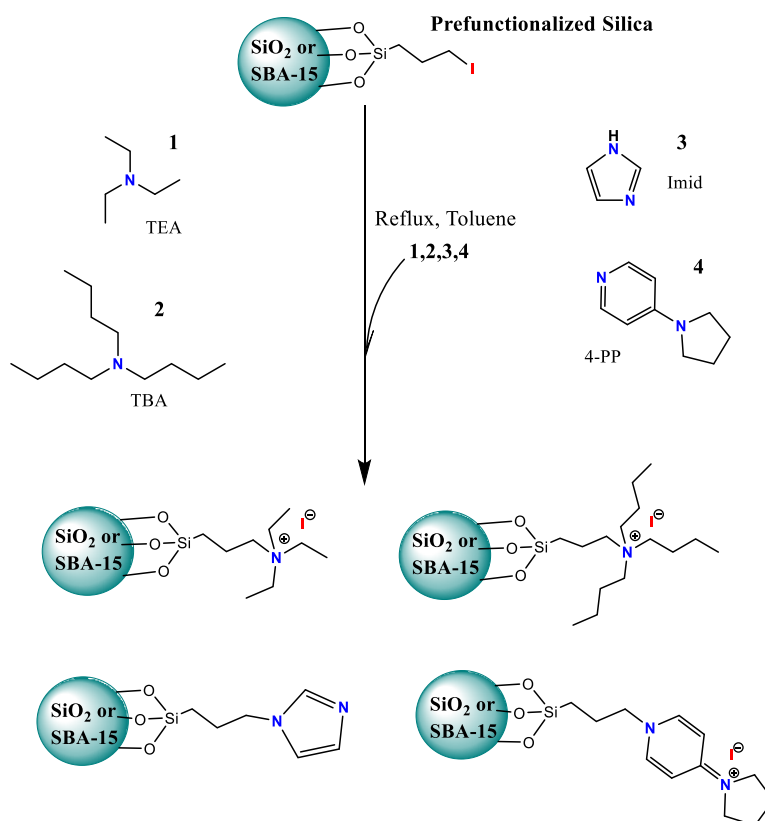

Figure 20. Overview of the catalyst preparation procedure.

4.1.2 Catalyst characterization

TEM images revealed surface morphologies of the supports and catalyst as shown in Figure 21. The commercial silica gel (Figure 21a) had an irregular porosity which is typical of amorphous materials, while the synthetized SBA-15 support exhibited very structured features of mesoporous materials with a uniform porosity and periodicity of the pores. The mesostructure was observed to stay intact when a metal dopant is introduced (Figures 21c and 21d). Furthermore, Zn/SBA-15(0.12) shows absence of metal particles on the surface, which evidences the good incorporation of Zn into the structure rather than on the surface. Otherwise, metal nanoparticles are evidenced on the surface of Zn/SBA-15(0.24) (Figure 21e), probably because of the high metal concentration used during the synthesis the excess was deposited on the surface. It was observed that the mesostructures of Zn/SBA-15(0.12) were well preserved after the immobilization of the catalytic species (Figure 21f).
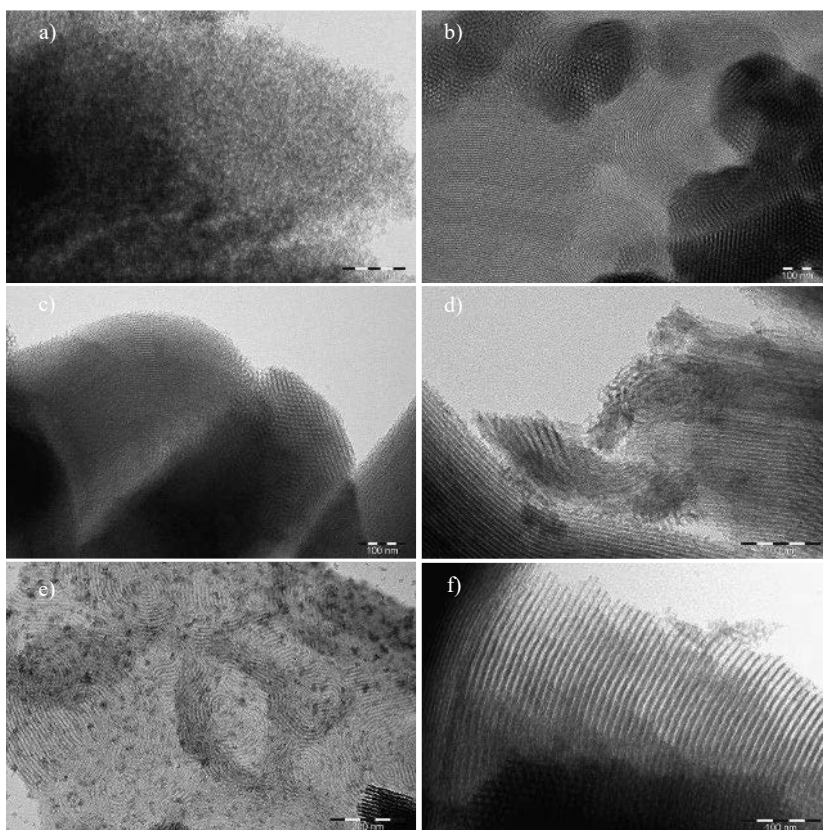

Figure 21. TEM images of the supports; a) Silica gel, b) SBA-15, c) Zn/SBA-15(0.12), d) Zn/SBA-15(0.24), e) Zn/SBA-15(0.24) (200 nm) and Zn/SBA-15(0.12)-4PPI.

A large difference between the surface areas of the commercial silica gel (460 m$^2 \cdot$g^{-1}) and the synthetized SBA-15 (948 m$^2 \cdot$g^{-1}) can be noticed in Table 9. This result is in line with the calculated total pore volume of SBA-15 which is almost two times larger than that of the commercial silica gel. The difference can be attributed to the large mesoporous volume of SBA-15. The average pore sizes of both supports were found to be around 7.8nm and 11.6nm for silica gel and SBA-15 respectively. The Zn/SBA-15(0.12) support shows almost an identical surface area as SBA-15. However, an important reduction of the surface area is observed when a 0.24 Zn/Si molar ratio is used instead, probably because of the deposition of metal nanoparticles on the surface as evidenced in the TEM images.

Table 9. Textural properties of the catalyst.

Catalyst	BET surface Area (m$^2 \cdot$g^{-1})	Average Pore size d$_p$ (nm)	Total pore volume V$_p$ (cm$^3 \cdot$g^{-1})	Micropore volume (cm$^3 \cdot$g^{-1})	Mesopore volume (cm$^3 \cdot$g^{-1})
SiO$_2$	460	7.8	0.76	0.11	0.65
SBA-15	948	11.6	1.41	0.29	1.12
Zn-SBA-15 (0.12)	999	11.9	1.53	0.29	1.24
Zn-SBA-15 (0.24)	675	11.3	0.97	0.12	0.85
SiO$_2$-Imid	348	6.1	0.45	0.06	0.39
SiO$_2$-TEAI	312	6.3	0.42	0.05	0.37
SiO$_2$-TBAI	290	5.7	0.36	0.04	0.32
SiO$_2$-4PPI	241	7.7	0.33	0.04	0.29
SBA-15-4PPI	479	11.4	0.76	0.12	0.64
Zn-SBA-15(0.12)-4PPI	296	11.4	0.50	0.07	0.43
Zn-SBA-15(0.24)-4PPI	276	10.9	0.43	0.06	0.37
Zn-SBA-15(0.12)- Imid	508	11.3	0.81	0.12	0.69
Zn-SBA-15(0.12)-TEAI	395	11.5	0.66	0.08	0.58
Zn-SBA-15(0.12)-TBAI	409	11.2	0.63	0.09	0.54

The textural properties of silica and SBA-15 supports are significantly reduced with the introduction of the catalytic species onto the surface. Lower surface areas, pore volumes and pore diameters were obtained for all the supported catalysts (Table 9). This can be attributed to the good anchoring of catalytic species into the internal pores of the supports and partially blocking the pore structure.
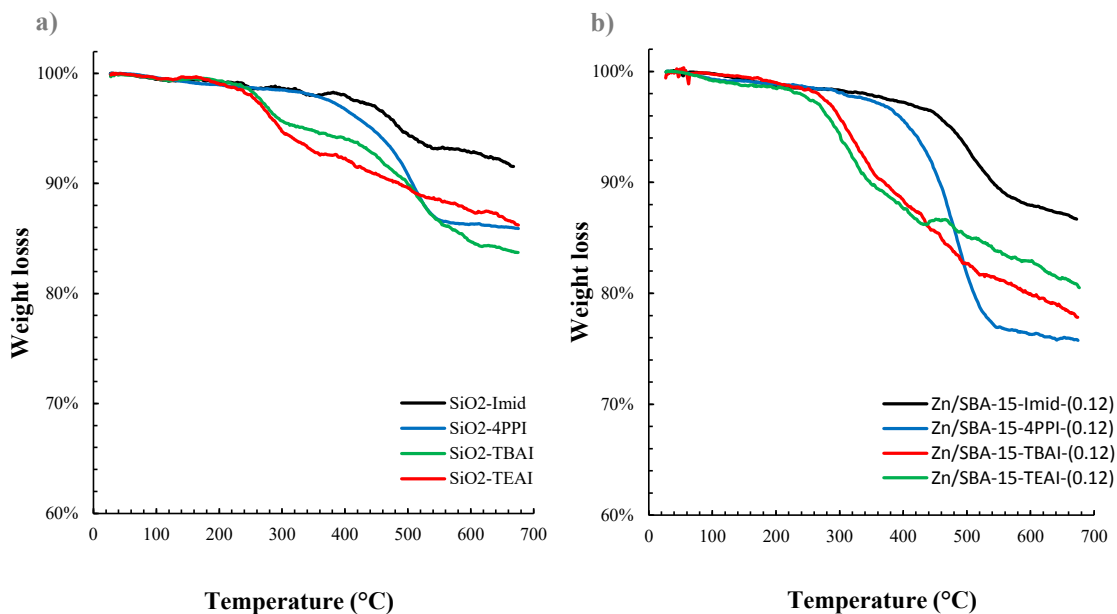

Figure 22. TGA curves of the catalytic materials; a) Silica gel supported b) SBA-15 supported.

Thermogravimetric analysis (TGA) of the samples (Figure 22) was used to determine their thermal stabilities as well as to estimate the amount of catalytic species attached to the supports. In Figure22a, the SiO_2-Imid and SiO_2-4PPI samples show a common decomposition temperature at around 300 °C with weight losses of 8% and 14% respectively. SiO_2-TBAI and SiO_2-TEA on the other hand, present lower thermal stabilities, with weight losses of 14% and 16% respectively starting at temperatures around 225°C. The same decomposition temperatures were observed for all catalytic species when supported in Zn/SBA-15 (Figure 22b), otherwise, it is evident when comparing Figure 22a and Figure 22b that larger amounts of catalytic species are attached on the surface of Zn/SBA-15. Larger weight losses are observed in all cases, presumably because Zn/SBA-15 possesses more available surface area for functionalization.

4.1.3 Catalyst activity

In a typical experiment, a mixture of epoxidized methyl oleate and the catalyst was placed in an autoclave reactor (Figure 8). Thereafter, the reactor was purged by flowing CO_2 three time and once the desired reaction temperature was attained, the reaction was started by introducing CO_2 at a constant pressure. Vigorous stirring was applied (1000 rpm).

Table 10. Activities of the synthetized catalysts.[a]

Entry	Catalyst	Substrate	Reaction time (h)	Conversion (%)	Selectivity (%)
1	SiO$_2$-Imid	EMO	8	18	19
2	SiO$_2$-ImidBr-OH	EMO	8	17	69
3	SiO$_2$-TEAI	EMO	8	23	93
4	SiO$_2$-TBAI	EMO	8	31	60
5	SiO$_2$-4PPI	EMO	8	24	99
6	SiO$_2$-TEAI	EMO	23	45	95
7	SiO$_2$-TBAI	EMO	23	42	94
8	SiO$_2$-4PPI	EMO	23	42	99
9	SBA-15-4PPI	EMO	23	57	99
10	Zn/SBA-15(0.12)-4PPI	EMO	23	66	90
11	Zn/SBA-15(0.24)-4PPI	EMO	23	63	96
12	Zn/SBA-15(0.12)-4PPI	EMO	32	75	91
13	Zn/SBA-15(0.12)-TEAI	EMO	23	54	90
14	Zn/SBA-15(0.12)-TBAI	EMO	23	55	97
15	Zn/SBA-15(0.12)-Imid	EMO	8	12	24
16	Zn/SBA-15(0.12)-4PPI[b]	EMO	23	47	99
16	Zn/SBA-15-4PPI-(0.12)[c]	EMO	23	76	75
17	Zn/SBA-15(0.12)-4PPI[d]	EMO	23	63	65
18	Zn/SBA-15(0.12)-4PPI	ECSO_FAME	23	47	85
19	Zn/SBA-15(0.12)-4PPI	ETO_FAME	23	57	60
20	Zn/SBA-15(0.12)-4PPI-(reuse1)	EMO	23	52	96

(a) Reaction conditions: epoxidized oil (50 g), catalyst (4 g), 30 bar CO_2, 140 °C, 1000 rpm. (b) 120°C. (c) 160°C. (d) H$_2$O= 2 gr

The catalytic activities of all supported catalytic species for the carbonation of epoxidized methyl oleate are reported in Table 10. Supported imidazole on both silica and mesoporous SBA-15 was tested (entry 1 and 15). This catalyst has been previously used [28] for the carbon dioxide cycloaddition of various alkene oxides with important catalytic activity. However, in the case of vegetable oils derivatives such as EMO poor performance was observed with nearly no catalytic activity. Although the hydroxyl functionalization of the imidazole on the catalyst surface (entry 2) slightly improved its performance by providing an extra source of HBDs [29], the conversion was still very low. TEA, TBA and 4-PP supported on silica (entry 3, 4 and 5) showed low catalytic activities as well. However, the conversion and yield were significantly improved when the reaction time was extended to 23h (entry 6, 7, 8). The TEA and TBA catalysts showed almost identical catalytic performance, the oxirane conversions were 45% and 42% respectively, while the yields of the carbonated product were 95% and 94% respectively. The conversion and yield obtained using SiO_2-4PPI (entry 8) were similar to those obtained for TEA and TBA.

The influence of large mesoporosity in the support is reported in Table 10. One of the most limiting factor when valorizing vegetable oils and their derivatives is presumed to be their size. Bulky substrates such as fatty acids and their methyl ester do not diffuse easily into microporous materials, which is the case for the vast majority of the high-performance catalysts in the market. Entries 8 and 9 compare the catalytic activities of 4-PP catalyst supported on commercial silica with low mesoporosity and on SBA-15 with larger pores. A moderate increase is observed in the conversion of epoxides when a mesoporous support such as SBA-15 is used, the selectivity of carbonate remains invariable at 99%. While the reason for this increase might be the presence of large pores in which the epoxidized methyl ester is more able to diffuse and react, it is also arguable that because of the larger surface area in the SBA-15-4PPI, more catalytic species are incorporated as evidenced in the TGA analysis (Figure 22), which contributes to a slightly better conversion by providing more active sites for the reaction. Thereafter, the influence of the support acidity was explored. It was found that doping the support with a metal improved the catalyst performance. The addition of Zn to the SBA support was found to increase the catalytic activity as reported in entry 10. 4-PP supported on Zn/SBA-15(0.12) presents 24% higher conversion of epoxides than 4-PP supported on commercial silica. This increase in efficiency results from the ability of the Zn atoms to assist and activate the oxirane group in the epoxidized methyl oleate for its opening. An increase in performance was also evidenced when Zn/SBA-15(0.12) was used as the support for TEA and TBA (entry 13

and 14). Otherwise, it seems that a further increase on the Zn/Si molar ratio in the structure of SBA-15 does not improved the efficiency as reported in entry 11. This behavior might be caused by the deposition of metal nanoparticles on the surface when higher metal concentrations are used as evidenced in the TEM analysis (Figure 21). As reported in Table 9, the Zn/SBA-15(0.24) support shows smaller available surface area than Zn/SBA-15(0.12).

The addition of water as an extra hydrogen bond donor source have been previously studied in the carbonation short-chain epoxides [30], [31] and epoxidized vegetable oils [32] in the presence of homogenous catalysts, indicating that the conversion of epoxides is improved if a small amount of water is present. Otherwise, it is clear from Table 10 that addition of water to the system does provide any increase in the conversion when compared to the water-free system (entry 10 and entry 17), possibly because of the deactivation of zinc-based catalysts reported in literature [30], [32]. Conversely, the selectivity decreased to 65 %,which is probably caused by a secondary hydrolysis reaction of the epoxide [33], which was confirmed in the IR-spectra of the samples by the presence of broad peak in the range of 3550-3200 cm^{-1} corresponding to OH functionalities.

Besides EMO, the fatty acid methyl esters (FAMEs) of cottonseed oil and tall oil were investigated using Zn/SBA-15(0.12)-4PPI under similar operation conditions (entries 18 and 19). A decrease in the catalytic performance was observed. The oxirane conversion and the carbonate yield were lower than those for EMO (entry 10). The reason might be the different composition of the FAME of cottonseed oil and tall oil. Both oils contain a high percentage of linoleic acid, which bears two double bonds functionalities in the same carbon chain rather than one as in oleic acid and hence their epoxidized derivatives are expected to have higher concentration of oxirane. Moreover, some impurities such as rosin acids and unsaponifiables are also present in those oils, which could contribute to catalyst deactivation and blockage of active sites.
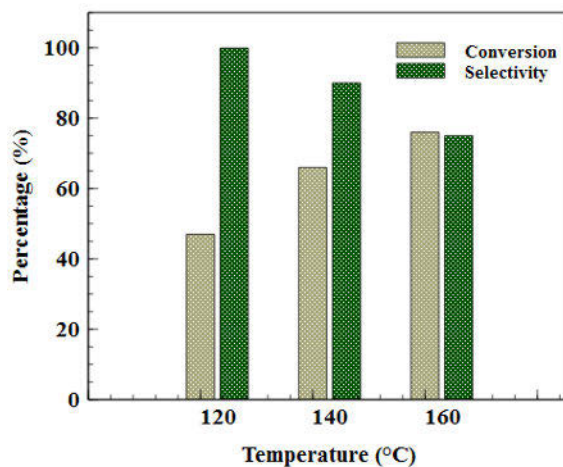
Figure 23. Effect of temperature on conversion and selectivity for the carbonation of EMO at 7.4 wt% of Zn/SBA-15(0.12)-4PPI catalyst, 1000 rpm and 23h.

The influence of the reaction temperature on the carbonation process using Zn/SBA-15(0.12)-4PPI was verified (Figure 23). A higher conversion of epoxized methyl oleate was obtained with increasing temperature, but the selectivity of the carbonated product decreased when the temperature was increased. Analogously, a lower reaction temperature resulted in lower conversion and higher selectivity. The carbon dioxide solubility is probably the main reason behind this result, because carbon dioxide is less soluble in the liquid phase at elevated temperatures [34], less carbon dioxide is available in the reaction medium, and in consequence the insertion step of carbon dioxide into the epoxide is slower.

Finally, the stability of Zn/SBA-15(0.12)-4PPI was tested by reusing the spent catalyst. The catalyst presented some deactivation as reported in Table 10 (entry 10 and 24). The reason was investigated using ICP-EOS and it was found that a small amount of iodine had leached from the catalytic species at every reused.

4.1.4 Reaction mechanism

As evidenced by our results and in the same line with previous works reported in literature [13], [35], the carbon dioxide cycloaddition to epoxide is mainly carried out by bifunctional catalysts and co-catalyzed systems, in which a cooperative acid-base mechanism takes place. The utilization of a Lewis acid metal centre have been demonstrated to enhance the reaction by proving a source of hydrogen bond donor. However, our experimental results showed that the

reaction can also proceed at slower rates in the absence of a Lewis acid metal centre as demonstrated in the carbonation experiments with silica supported catalyst in the absence of Zn (Table 10; entry 1-9). These results are in line with some previous reports [25]-[26] where it has been proposed, that the OH species on the silica surface can act as Lewis acid to synergistically activate the oxirane ring for its opening. Based on these considerations, a plausible molecular mechanism is proposed in Figure 24. In the first step, the oxirane ring is adsorbed into the surface either by Lewis acid metal centre or OH groups on the silica support, this results in the activation of the oxirane ring by polarization. Then the active epoxide is attacked though the less hindered carbon by the halide anion of the catalytic specie to produce a ring-opening complex. Thereafter, the CO_2 insertion proceeds and a new carbonate intermediate is formed on the surface. Finally, ring closure results in the formation of cyclic carbonate, which is released from the surface.
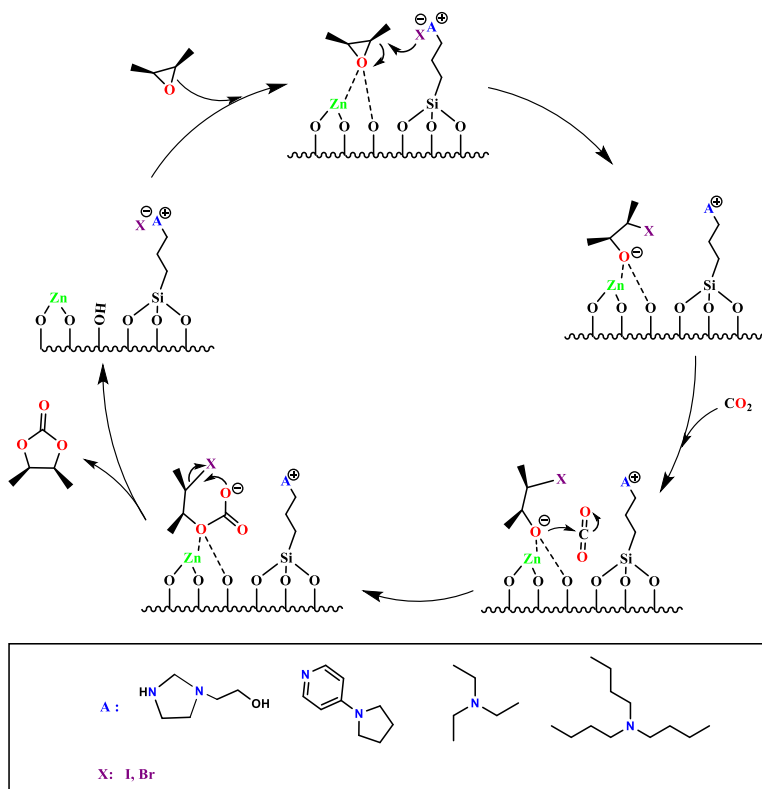

Figure 24. Proposed surface reaction mechanism for the carbonation reaction of EMO with various nucleophilic catalysts attached to a Zn-doped support.

5. Aminolysis

The aminolysis of carbonated methyl oleate was investigated using different amines. Thermal analysis and kinetics studies were conducted.

5.1 Kinetics investigations

The aminolysis reaction of carbonated vegetables oils with amines was investigated using carbonated methyl oleate and n-butylamine as a model system to produce urethane. The reaction kinetics was investigated experimentally and kinetic modelling was conducted. Moreover, thermal analysis was performed using the C80 Setaram calorimeter to determine the reaction enthalpies of the aminolysis system.
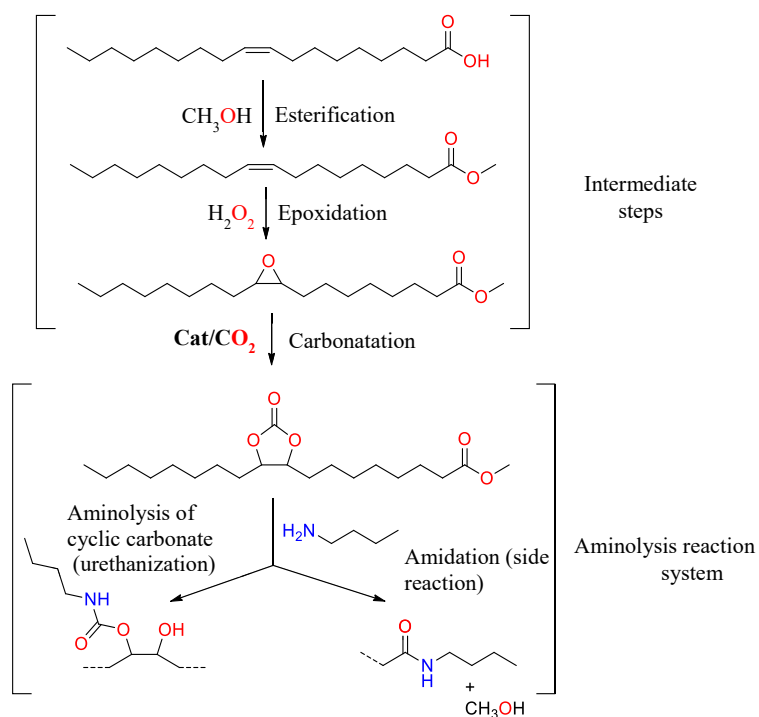

Figure 25. Strategy for the production of the non-isocyanate urethane from oleic acid as a model system.

In a typical aminolysis experiment, the carbonated methyl oleate (CMO) was placed in the reactor and once the target temperature was reached, the n-butyl amine was introduced dropwise using a peristaltic pump. Prior to the aminolysis reaction, the initial oleic acid underwent

esterification, epoxidation and carbonation to afford carbonated raw material for the aminolysis reaction (the process steps are shown in Figure 25).

5.1.1 Characterization of products and intermediates

The FTIR spectra of the intermediates and final urethane methyl oleate (UMO) are displayed in Figure 26. Firstly, the conversion of the carboxylic acid group in the oleic acid (OA) through esterification with methanol was confirmed by the appearance of the ester band at $1710 \, \text{cm}^{-1}$ in the methyl oleate (MO) spectra, residual carboxylic acid is observed at $1738 \, \text{cm}^{-1}$. Then, the epoxidation of the methyl oleate is evidenced by the disappearance of the C=C-H stretching in the range $3000\text{-}3050 \, \text{cm}^{-1}$ and the appearance of bands between $815 \, \text{cm}^{-1}$ and $950 \, \text{cm}^{-1}$ corresponding to the C-O-C stretching of oxirane ring in the epoxidized methyl oleate sample (EMO). Carbonated methyl oleate (CMO) shows a strong band at $1800 \, \text{cm}^{-1}$ corresponding to the carbonate group, furthermore the absence of absorption bands of the epoxide group between 815 and $950 \, \text{cm}^{-1}$ confirms the good conversion of epoxides. Finally, in the aminolysis process, the decrease of the signal $1800 \, \text{cm}^{-1}$ evidences the consumption of the carbonated group. The formation of urethane is confirmed by the characteristic bands at $1720 \, \text{cm}^{-1}$ and $1647 \, \text{cm}^{-1}$. Moreover, OH functionalities bands appears between $3550 \, \text{cm}^{-1}$ and $3200 \, \text{cm}^{-1}$ due to the hydroxyl formed during the ring-opening of the cyclic carbonate.
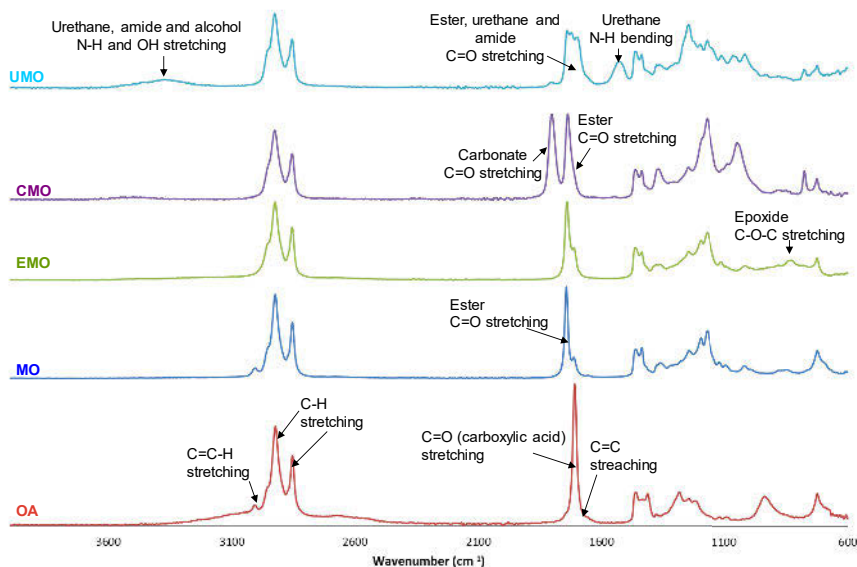

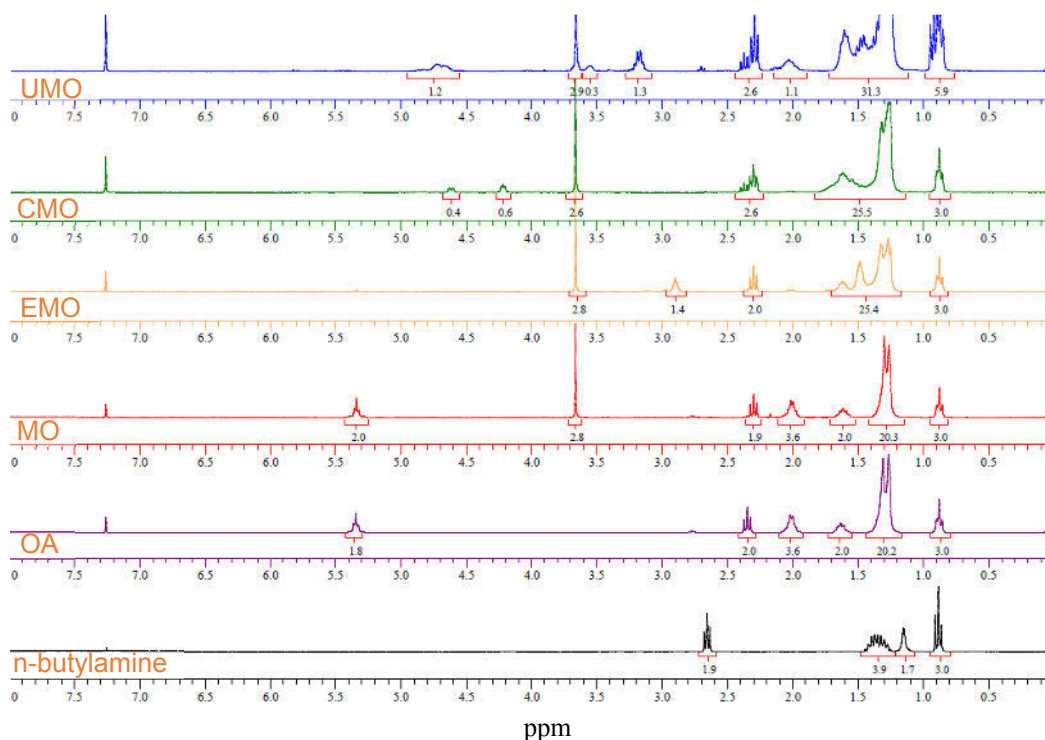Figure 26. FTIR-spectra for OA, MO, EMO, CMO and UMO.

Figure 27. ^{1}H-NMR for OA, MO, EMO, CMO and UMO.

The formation of intermediates and the final product was also investigated by proton nuclear magnetic resonance spectroscopy (^{1}H-NMR), the spectra are displayed in Figure 27. The quantitative conversion of OA to MO is confirmed by the emergence of the corresponding signal of the methyl ester group at 3.66 ppm as well as by the displacement of the signal of methylene group in α-position to acid group from 2.34 ppm to 2.29 ppm. The spectrum of EMO revealed that the signal at 5.34 ppm related to the carbon-carbon double bonds disappeared. The epoxide formation was confirmed by the characteristic signal displayed at 2.90 ppm. The signals between 4.40 and 4.95 ppm assigned to the cyclic carbonated are displayed in the spectra of CMO. Then, during the aminolysis experiments the conversion of carbonated groups is observed through the disappearance of the cyclic carbonate signals at 4.22 ppm and 4.61 ppm. In the range of 4.8–5.2 ppm, the broad signal is assigned to protons of NH and those in alpha position to the oxygen of the urethane function. Protons in α-position of the nitrogen arised at 3.16 ppm. The signal at 3.55 ppm is ascribed to protons in α-position of hydroxyl groups.

5.1.2 Calorimetry analysis of the aminolysis reaction

The reaction enthalpies of the aminolysis reaction and the amination side reaction were investigated using the C80 Seratam calorimeter. The evolution of the recorded heat-flow rates as function of time is depicted in Figure 28. The overall energy released due to urethane and to amide formation at 60 °C is displayed in Figure 28a, while Figure 28b stands only for the heat released during the formation of urethanes at 60 °C.

By integrating the curves in Figure 28a, the overall enthalpy of the reaction system (amidation + aminolysis) was found to be -23.90 kJ·mol^{-1} of the carbonated group. Thereafter, the integration of the heat-flow rates shown Figure 28b provides the enthalpy due to the formation of the urethanes, which was found to be -18.92 kJ·mol^{-1}. Thus, the enthalpy of amidation is -5.02 kJ·mol^{-1}. These results of reaction enthalpies indicate that the aminolysis of carbonated methyl oleate is not very exothermic. If the reaction enthalpy during the real polymerization process of polyurethane is assumed to be proportional to the amount of carbonated functionalities, for a typical vegetable oil molecules where in average three carbonated groups are present, the overall reaction enthalpy should be approximately 71 kJ·mol^{-1}, which represents a relatively low exothermicity.
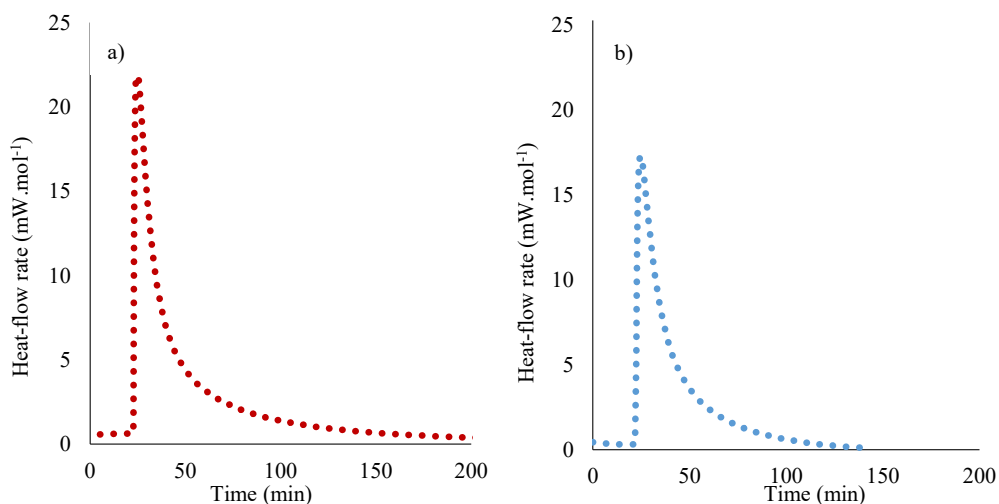

Figure 28. a) Heat profiles for CMO and n-butylamine system at 60 °C. b) Heat profile for the urethane formation at 60°C.

5.1.3 Kinetic modelling of the aminolysis reaction

In order to monitor the evolution of the reaction system in a quantitative way, samples were analyzed by FTIR spectroscopy. Carbonated groups and ester group concentrations were calculated from the samples spectra using calibration curves.
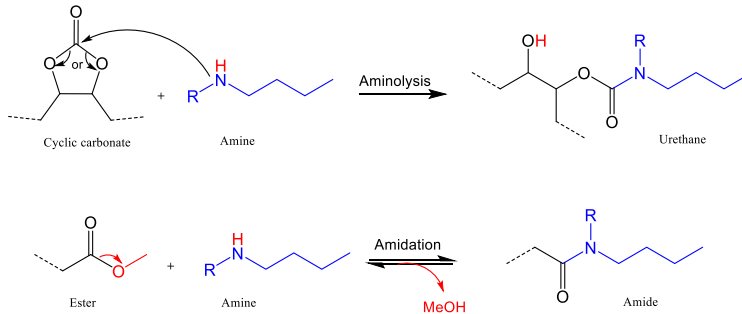

Figure 29. Reaction scheme for aminolysis and amidation reactions.

As illustrated in Figure 29, the system consists of the main reaction, which is the aminolysis of the carbonated group, and a side reaction, the amidation of carboxylic acid group. The aminolysis reaction was considered as an elementary reaction, while the amidation reaction is known to be a reversible one. The reaction rates were expressed as it follows,

$$r_{Aminol} = k_{Aminol} \cdot c_{carbonated} \cdot c_{nBA} \tag{12}$$

$$r_{Amid} = k_{Amid} \cdot \left(c_{ester} \cdot c_{nBA} - \frac{c_{amide} \cdot c_{MeOH}}{K_c} \right) \tag{13}$$

where r_{Aminol} and r_{Amid} represent the rates of the aminolysis and the amidation steps respectively. the parameter k_{Aminol} and k_{Amid} are the rate constants of the aminolysis and the amidation reactions and $c_{carbonated}$, c_{ester}, c_{nBA}, and c_{amide} denote the concentrations of carbonated group, ester group, n-butyl amine, and amide group, respectively. K_c is the equilibrium constant for the amidation reaction.

The temperature dependence of K_c was expressed by the law of van 't Hoff,

$$K_c(T) = K_c(T_{ref}) \cdot \exp\left(\frac{-\Delta H_{Amid}}{R} \cdot \left(\frac{1}{T} - \frac{1}{T_{ref}}\right)\right) \tag{14}$$

Where T and T_{Ref} represent the reaction temperature and reference temperature (70 °C). R is the universal gas constant and ΔH_{Amid} is the enthalpy of the amidation reaction, which was determined to be -5.02 kJ·mol^{-1} with calorimetric experiments.

A constant volumetric flow rate of the amine was applied during the experiments and thus the change of the reaction volume during the course of the reaction is assumed to be the volumetric flow rate,

$$\frac{dV_r}{dt} = Q_{feed} \quad \text{for } t < t_{add} \quad \text{and} \quad \frac{dV_r}{dt} = 0 \quad \text{for } t > t_{add} \tag{15}$$

where Q_{feed} is the volumetric flow rate, t_{add} is the addition time and V_r is the volume of the reaction mixture. Equation (15) was used to simulate the evolution of the reactor volume.

The mass balances of all the components in the reaction system can be expressed as

$$\frac{dc_{carbonated}}{dt} = -r_{A\min ol} - c_{carbonated} \cdot \frac{Q_{feed}}{V_r} \tag{16}$$

$$\frac{dc_{nBA}}{dt} = -(r_{A\min ol} + r_{Amid}) + (c_{amide-feed} - c_{amide}) \cdot \frac{Q_{feed}}{V_r} \tag{17}$$

$$\frac{dc_{UMO}}{dt} = r_{A\min ol} - c_{UMO} \cdot \frac{Q_{feed}}{V_r} \tag{18}$$

$$\frac{dc_{ester}}{dt} = -r_{Amid} - c_{ester} \cdot \frac{Q_{feed}}{V_r} \tag{19}$$

$$\frac{dc_{amide}}{dt} = r_{Amid} - c_{amide} \cdot \frac{Q_{feed}}{V_r} \tag{20}$$

$$\frac{dc_{MeOH}}{dt} = r_{Amid} - c_{MeOH} \cdot \frac{Q_{feed}}{V_r} \tag{21}$$

where c_{UMO} and c_{MeOH} are the concentration of the urethane methyl oleate product and methanol, respectively.

The estimation of the kinetic parameters was performed using the software ModEst [24]. The ordinary differential equation systems formed by equations (15)-(21) was solved by an ODESSA algorithm based on the backward difference method.

The experimental concentration of the carbonated group and the ester group were the observables. The objective function (OF) was minimized with a combined simplex-Levenberg-Marquardt algorithm.

$$OF = \sum (C_{i,\exp} - C_{i,sim})^2 \tag{22}$$

where $C_{i,exp}$ is the experimental concentration and $C_{i,sim}$ is the concentration simulated by the mathematical model.

The reliability of the model to describe the experimental data was examined with the following coefficient of explanation,

$$R^2 = 1 - \frac{\sum (C_{i,\exp} - C_{i,sim})^2}{\sum (C_{i,\exp} - \overline{C}_{i,\exp})^2} \tag{23}$$

where $\overline{C}_{i,\exp}$ is the average value of the experimental concentration.

To minimize the correlation between the activation energy and the pre-exponential factor, the reaction rate constants were expressed using a modified Arrhenius equation,

$$k_i(T) = k_i(T_{ref}) \cdot \exp\left(\frac{-E_a}{R} \left(\frac{1}{T} - \frac{1}{T_{ref}} \right) \right) \tag{24}$$

where, k_i is reaction rate constant, E_a is the activation energy, T is the reaction temperature, T_{Ref} is the reference temperature and R is the universal gas constant.

Some experimental results of the kinetic modelling are presented in Figure 30. A rather good fit of the mathematical model to the experimental data is observed with a degree of explanation exceeding 90%. The concentrations of amide and urethane were simulated and plotted as well. The contour plots for the estimated kinetic and activation energy constants for both reactions

are illustrated in Figure 31. It is clear that the minimum of the objective function was reached in the parameter estimation.
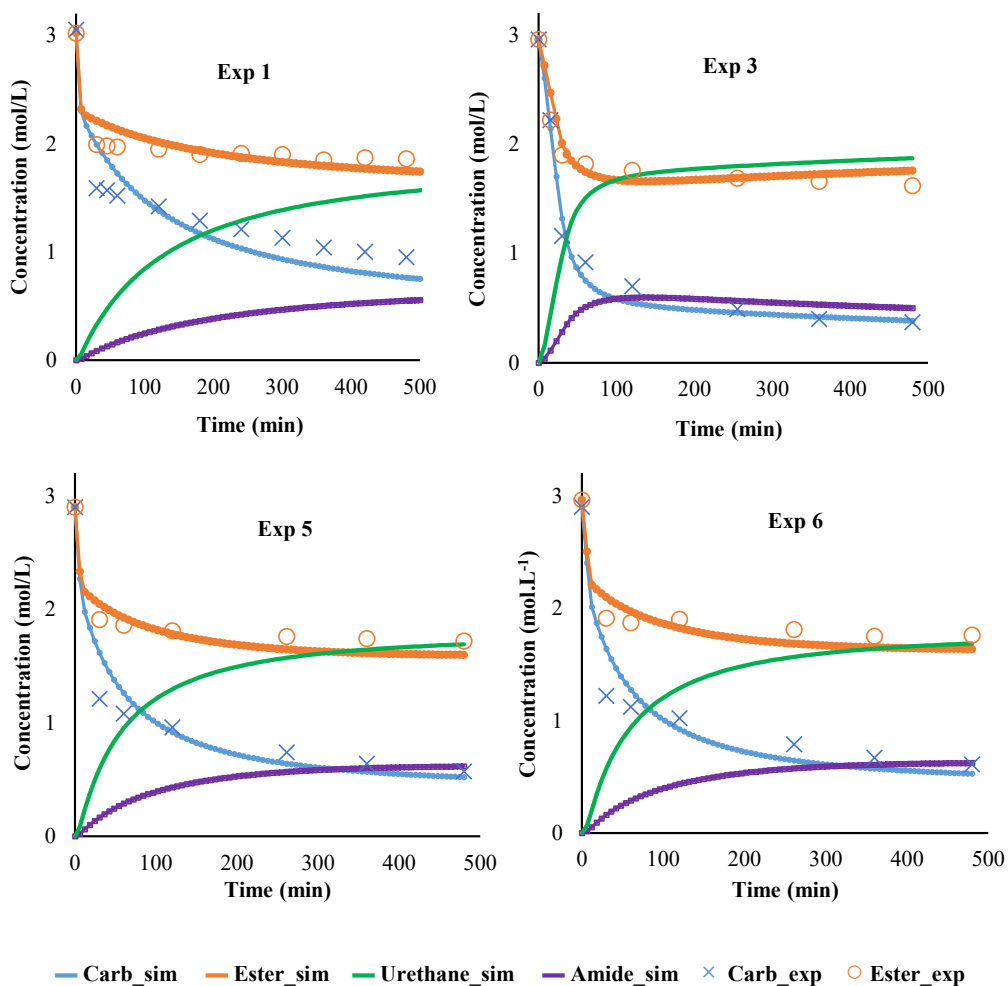

Figure 30. Fit of the mathematical model to the experimental data for the aminolysis of carbonated of methyl oleate with n-butylamine.

The values of the estimated parameters and their standard deviations are reported in Table 11. The standard errors were estimated within the confidence interval of 95%. All the standard deviations are low for the kinetic constants. Although, for the equilibrium constant of the amidation reaction (K_C), a somewhat high value of the standard deviation was observed (78%). Otherwise, the parameter estimation results are reasonable, considering the complexity of the system.
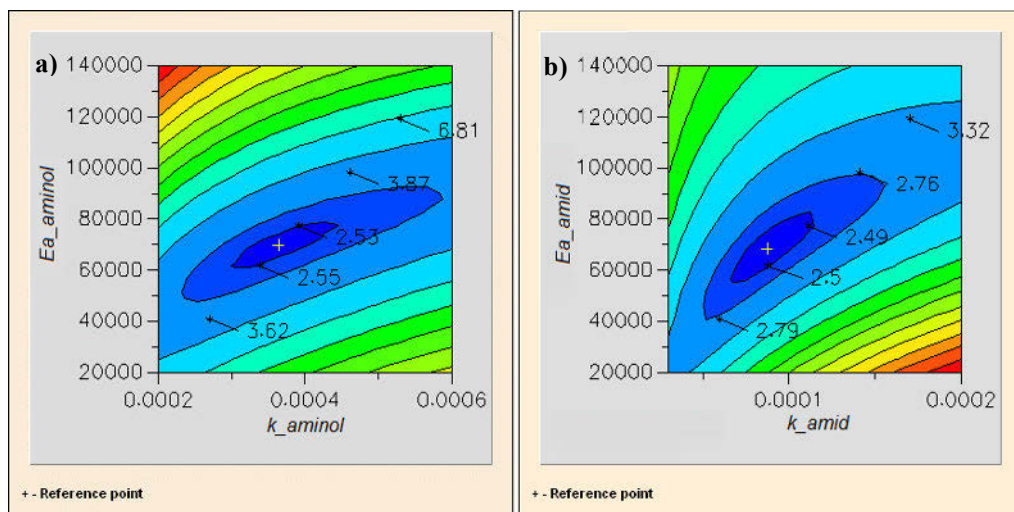
Figure 31. Contour plot of kinetic parameters for the aminolysis (a) and amidation (b).

Table 11. Parameter estimation results for aminolysis of carbonated methyl oleate with n-butylamine at $T_{ref} = 70$ °C.

	Estimated parameter	Est. Relative Std Error (%)
k_{Amid}	8.76E-05	24.5
Ea_{Amid}	6.81E+04	16
k_{Aminol}	3.64E-04	15.2
Ea_{Aminol}	6.98E+04	9.8
K_C	3.03	98.2

Units: $k_i = $ (L·mol^{-1}·s^{-1}); $Ea_i = $ (J·mol^{-1}) ; K_C at 70 °C

5.2 Structure and reactivity

Steric hindrance in the aminolysis reaction system was investigated by varying the length of the amine used. For this purpose, kinetic models of the aminolysis reaction using butylamine (BA), methylbutylamine (MBA), ethylbutylamine (EBA) and dibutylamine (DBA) as reagents was performed. A linear free energy relationship was explored by linking the amine substituents to their reactivities towards the aminolysis.

The experiments were performed in batch mode under isothermal conditions. The carbonated methyl oleate was placed in the reactor and heated to a target temperature under mechanical stirring (500 rpm). Thereafter, the amine was added to start the reaction. Prior to the addition, the amine was preheated to the reaction temperature. Different reaction temperatures were utilized depending on the amine because of their different levels of reactivity.

5.2.1 Kinetic modelling using different amines

Equations 12 and 13 were used to express the reaction rates of aminolysis and amidation, respectively. The equilibrium constant of the amidation reaction was presumed to be temperature-independent within the studied temperature range for each amine.

The mass balances of the components were expressed as

$$\frac{dc_{carbonated}}{dt} = -r_{A\min ol} \tag{25}$$

$$\frac{dc_{nBA}}{dt} = -(r_{A\min ol} + r_{Amid}) \tag{26}$$

$$\frac{dc_{UMO}}{dt} = r_{A\min ol} \tag{27}$$

$$\frac{dc_{ester}}{dt} = -r_{Amid} \tag{28}$$

$$\frac{dc_{amide}}{dt} = r_{Amid} \tag{29}$$

$$\frac{dc_{MeOH}}{dt} = r_{Amid} \tag{30}$$

All the numerical operations were performed using the software ModEst [24]. The ordinary differential system formed by equations 25-30 was solved numerically by the ODESSA algorithm integrated in the ModEst Software. Non-linear regression was used to estimate the parameters.

The minimum of the error squares between experimentally recorded and predicted (equation 22) concentrations was searched with a combined simplex-Levenberg-Marquardt algorithm. The ability of the mathematical model to simulate the experimental data was evaluated by the coefficient of determination (equation 23). The modified Arrhenius expression (equation 24) was used in order to suppress the correlation between the pre-exponential factor and the activation energy.

A summary of the modelling results for the different amine systems is displayed in Figure 32 and Figure 33. Overall, an excellent fit of the models to the experimental data was obtained. The degree of explanation for the four models was found to be 99.7%, 99.50%, 98.30 and 99.09% for t butylamine, methybutylamine, ethylbutylamine and dibutylamine, respectively.
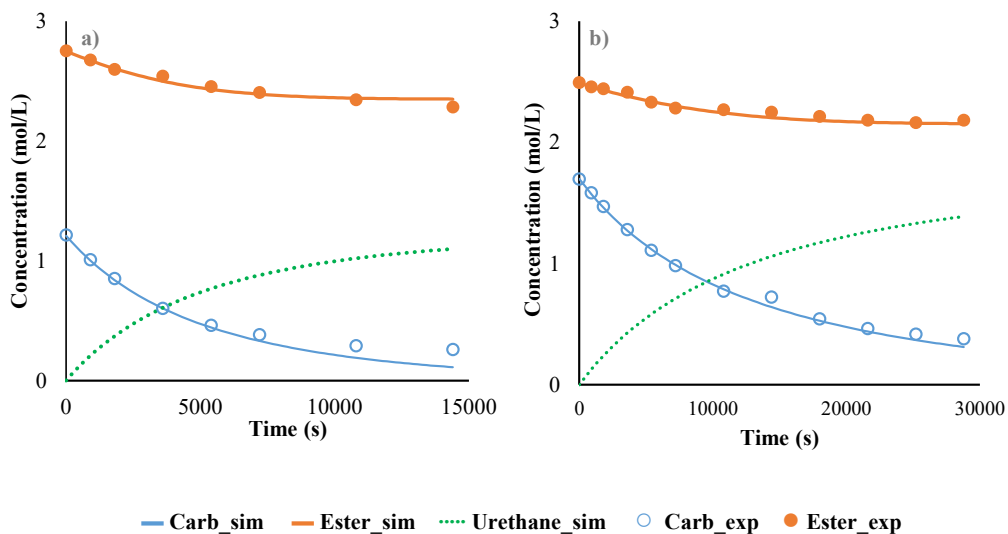

Figure 32. Fit of the mathematical model for the aminolysis reaction of carbonated methyl oleate. a) n-butylamine system at 60 °C, b) methylbutylamine system at 90 °C.
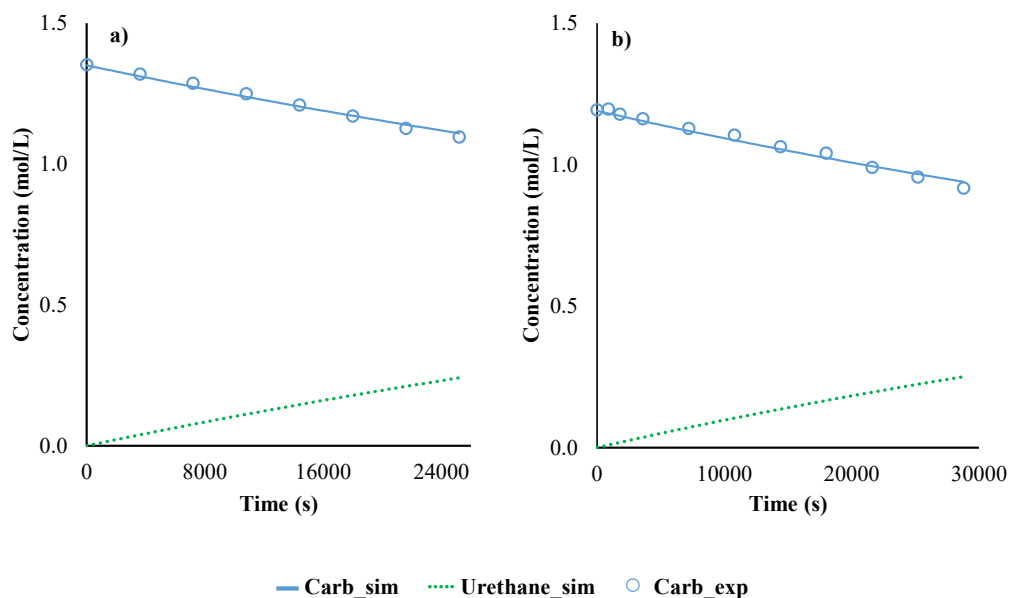
Figure 33. Fit of the mathematical model for the aminolysis reaction of carbonated methyl oleate. a) ethyl butyl amine system at 109 °C, b) dibutylamine system at 130 °C.

If Figures 33 and 33 are compared, it is clear that the BA and MBA reaction system possess more rapid kinetics than those of EBA and DBA. Furthermore, during the experiments it was observed that the amidation reaction was extremely slow in the EBA and DBA reaction systems and therefore it was discarded during the kinetic modeling stage.

5.2.2 Effect of the amine substituent in the aminolysis reaction rate

The aminolysis reaction rate constant for the BA, MBA and DBA systems are shown at different temperatures in Figure 34. It is evident that the aminolysis rate of reaction increases in the following order: $R_{Aminolysis\ by\ BA} > R_{Aminolysis\ by\ MBA} > R_{Aminolysis\ by\ DBA}$ at any temperature. Otherwise at 109 °C, the aminolysis reaction rate increase in the following way $R_{Aminolysis\ by\ BA} > R_{Aminolysis\ by\ MBA} > R_{Aminolysis\ by\ EBA} > R_{Aminolysis\ by\ DBA}$. As the length of the amine substituent increases more steric hindrance is encountered and thus the kinetics of the aminolysis reaction decreases.
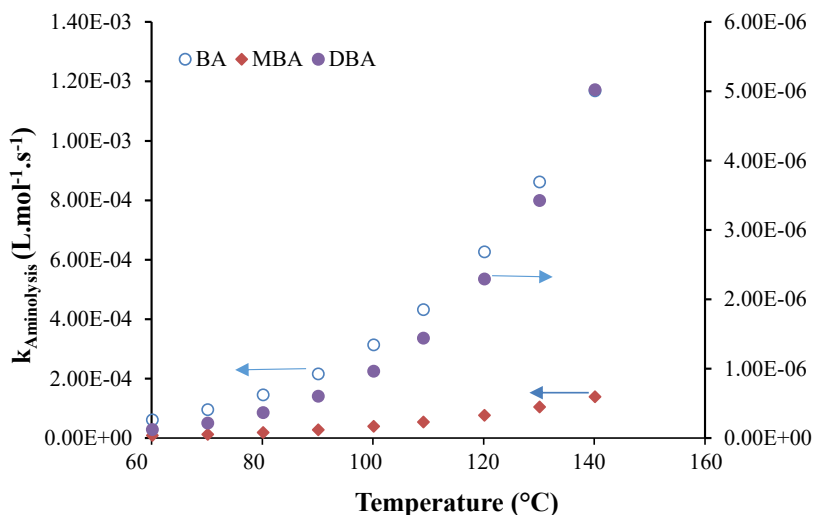
Figure 34. Evolution of the aminolysis rate constants at different temperatures and substituents.

The following linear free energy relationship (LFER) was established to predict the influence of the amine substituent on the aminolysis reaction rate,

$$lg(k_x) = a \cdot b_x + c \tag{31}$$

where k_x is the aminolysis reaction kinetic rate constant, b_x is a coefficient dependent on the amine substituents; –H (for BA), -Me (for MBA), -Et (for EBA) and –Bu (for DBA), and a and c are temperature dependent constants. The values of b_x are reported in Table 12. A value of 3 was assumed for the Bu- substituent because of better statistical results.

Table 12. Values of b_x.

Substituents	b_x
H-	0
Me-	1
Et-	2
Bu-	3

Equation 31 was applied using the kinetic rates obtained during the kinetic modelling and the b_x values reported in Table 11. The values of the constant a and b are obtained directly from the plotted curves in Figure 35 at different temperatures. It is clear from the curves that there is a correlation between the reactant length and the kinetics of the aminolysis reaction system.
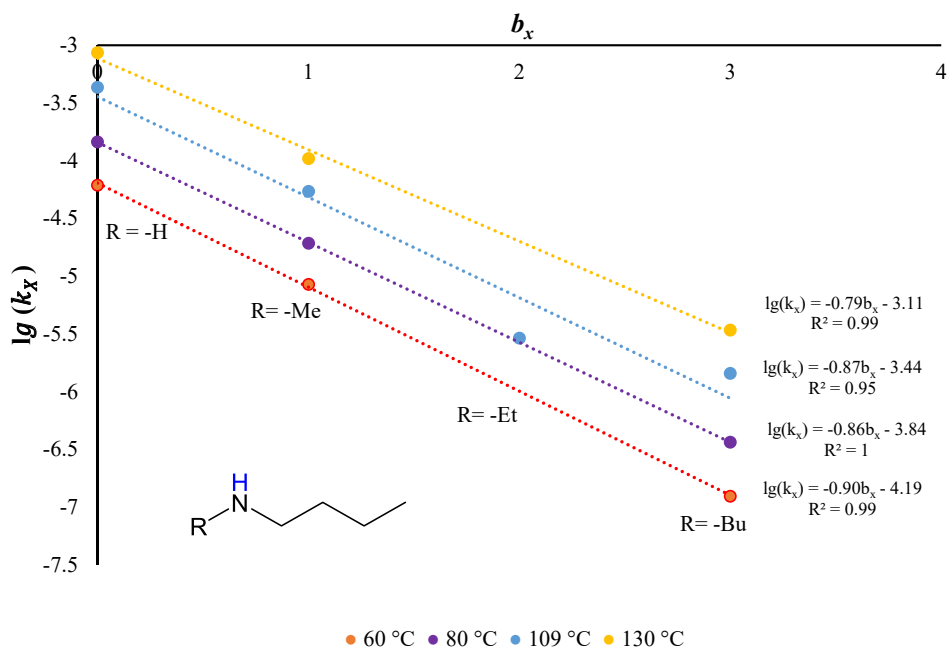

Figure 35. Application of equation (31) to the aminolysis system.

6. Conclusions

The present scientific work contributes to the development of non-isocyanate polyurethane production from vegetable oil and carbon dioxide feedstock by providing optimization of the early reaction steps and thermally safer production of intermediates. Moreover, thermal analysis of the aminolysis reaction and kinetic modelling was systematically conducted in order to get better understanding of the system.

The epoxidation step, which is presumed to be the most exothermic reaction of the pathway for the production of polyurethane from vegetable oils, was investigated from the viewpoint of process safety. Thermal risk assessment of various epoxidation systems was conducted. It was concluded that direct epoxidation with hydrogen peroxide in the presence of a metal oxide catalyst such as γ-Al_2O_3 shows lower probabilities of thermal runaway than the classical Prileschajew method, which is the currently dominating production technology of epoxidized vegetable oils. The main advantage of the Prileschajew method is the rather good yield of epoxide; otherwise the technology has multiple problematic issues such as post-reaction organic waste, utilization of corrosive acids and high exothermicity.

All of this problems are circumvented in the direct epoxidation with hydrogen peroxide, which was demonstrated to be a less exothermic system and it does not require the utilization of carboxylic acids as reaction carriers. The efficiency of the direct epoxidation process was investigated in detail, and it was found that semi-batch reactor technology gives the best results in terms of double bond conversion and epoxide yields; very little ring opening reactions were observed, probably due to the low acidity of the reaction mixture compared to the Prileschajew system. A kinetic model based on a plausible reaction mechanism was established and a rather good description of the system was achieved with the model.

Several heterogeneous catalysts were synthetized by propyl linkage methods and screened for the carbonation process. A variety of catalytic species were anchored to a silica-based support. It was found that when the catalytic species is attached to molecular sieves such as SBA-15, an improved level of the epoxide conversion was achieved, probably because of larger pores and larger available surface areas. The influence of the Lewis acidity was investigated by doping the silica support with a metal (Zn). An increase in the conversion was evidenced when the support was doped with Lewis metal centre. Otherwise, it was observed that increasing the amount of doped metal does not provide any further improvement. A low Zn/Si molar ratio in

the support is sufficient to obtain a better catalyst performance. Some other effects were investigated such as temperature, presence of water and the utilization of different epoxidized vegetables oils. Supported 4-pyrrolydinpyrine supported on Zn-SBA-15(0.12) was found to be the most active heterogeneous catalyst among the screened ones. Overall, a reasonable epoxide conversion and an excellent selectivity of the carbonated product were obtained.

The aminolysis step was investigated using carbonated methyl oleate and n-butyl amine as a model system. Calorimetric experiments were conducted to reveal the reaction enthalpies of the system. The enthalpies aminolysis and amidation were found to be negatives and of low values, indicating weakly exothermic reactions. Kinetic modeling of the reaction system was performed and a rather good agreement between the mathematical model and the experimental data was achieved. Furthermore, the aminolysis reaction was found to be structure sensitive. The length of the amine was linked to the aminolysis rate. This effect was explained through a linear free energy relationship (LFER) with the amine substituent and their respective reaction rates.

This work brings a clearer understanding of the reaction pathway for the production of NIPUs from vegetable oils and carbon dioxide feedstock by providing essential data of kinetics and thermal characteristics of the intermediate and final reaction steps.

Notation

$\hat{C}_{PR}$	specific heat capacity of the reaction mixture
C/c	concentration
Ea	activation energy
ΔH	reaction enthalpy
K_c	equilibrium constant of the amidation reaction
k	reaction rate constant
m_R	reaction mixture mass
m_{cat}	catalysts mass
q_r	heat release rate due to chemical reaction
R^2	coefficient of determination
R	universal gas constant
R_i	reaction rate
r_i	catalytic reaction rates
r'_i	non-catalytic reaction rates
T/T_p	reaction temperature
T_{ref}	reference temperature
ΔT_{ad}	adiabatic temperature rise
ΔTMR_{ad}	time to maximum rate under adiabatic conditions
t	time
V	volume
V'/Q_{feed}	volumetric flow rate
$\alpha, \beta, \gamma, \omega$	merged rate parameters in equation rates (3) and (4)
β	ARSST electrical heating rate
ρ	density
τ_0	ratio between initial volume-to-volumetric flow rate
$*$	surface site

Subscripts and superscripts

Amid	amidation
Aminol	aminolysis
Add	addition

B	bulk
Exp	experimental
Sim	simulation
i, j	component index
L	liquid
0	inlet or initial quantity

Abbreviations

ARSST	advanced reactive system screening tool
AA	acetic acid
BA/nBA	butylamine
CVO	carbonated vegetable oil
CMO	carbonated methyl oleate
DB	component with a double bond, e.g. fatty acid ester
DBA	dibutylamine
EVO	epoxidized vegetable oil
EMO	epoxidized methyl oleate
EP	epoxidized product
EBA	ethylbutylamine
FA	formic acid
FAME	fatty acid methyl ester
GHG	greenhouse gas
HP	hydrogen peroxide
HBD	hydrogen bon donor
I	intermediate
Imid	imidazole
LSO	linseed oil
LFER	linear free energy relationship
MO	methyl oleate
MBA	methylbutylamine
NIPU	non-isocyanate polyurethane
OA	oleic acid
OF	objective function
PU	polyurethane

RO	ring opening reaction
TOFA	tall oil fatty acid
TEA	triethylamine
TBA	tributylamine
UMO	urethane methyl oleate
VO	vegetable oil
W	water

Acknowledgments

Johan Gadolin
Process Chemistry Centre

References

[1] A. Pattiya, 'Fast pyrolysis', in *Direct Thermochemical Liquefaction for Energy Applications*, Elsevier, 2018, pp. 3–28.

[2] F. Cherubini, 'The biorefinery concept: Using biomass instead of oil for producing energy and chemicals', *Energy Convers. Manag.*, vol. 51, no. 7, pp. 1412–1421, Jul. 2010, doi: 10.1016/j.enconman.2010.01.015.

[3] C. Briens, J. Piskorz, and F. Berruti, 'Biomass Valorization for Fuel and Chemicals Production -- A Review', *Int. J. Chem. React. Eng.*, vol. 6, no. 1, May 2008, doi: 10.2202/1542-6580.1674.

[4] R. Vicente and S. Mata, 'Chapter 7 - Zinc-Mediated Synthesis of Heterocycles', in *Advances in Transition-Metal Mediated Heterocyclic Synthesis*, D. Solé and I. Fernández, Eds. Academic Press, 2018, pp. 285–310.

[5] D. Chery, V. Lair, and M. Cassir, 'Overview on CO2 Valorization: Challenge of Molten Carbonates', *Front. Energy Res.*, vol. 3, 2015, doi: 10.3389/fenrg.2015.00043.

[6] Nathalie THYBAUD and David LEBAIN, 'Panorama des voies de valorisation du CO2', ALCIMED, ADEME.

[7] G. T. Howard, 'Biodegradation of polyurethane: a review', *Int. Biodeterior. Biodegrad.*, vol. 49, no. 4, pp. 245–252, Jun. 2002, doi: 10.1016/S0964-8305(02)00051-3.

[8] M. Bähr and R. Mülhaupt, 'Linseed and soybean oil-based polyurethanes prepared via the non-isocyanate route and catalytic carbon dioxide conversion', *Green Chem.*, vol. 14, no. 2, p. 483, 2012, doi: 10.1039/c2gc16230j.

[9] G. Lligadas, J. C. Ronda, M. Galià, and V. Cádiz, 'Novel Silicon-Containing Polyurethanes from Vegetable Oils as Renewable Resources. Synthesis and Properties', *Biomacromolecules*, vol. 7, no. 8, pp. 2420–2426, Aug. 2006, doi: 10.1021/bm060402k.

[10] D. P. Pfister, Y. Xia, and R. C. Larock, 'Recent Advances in Vegetable Oil-Based Polyurethanes', *ChemSusChem*, vol. 4, no. 6, pp. 703–717, 2011, doi: https://doi.org/10.1002/cssc.201000378.

[11] I. Javni, D. P. Hong, and Z. S. Petrovic, 'Soy-based polyurethanes by nonisocyanate route', *J. Appl. Polym. Sci.*, vol. 108, no. 6, pp. 3867–3875, Jun. 2008, doi: 10.1002/app.27995.

[12] A. Farhadian, A. Ahmadi, I. Omrani, A. B. Miyardan, M. A. Varfolomeev, and M. R. Nabid, 'Synthesis of fully bio-based and solvent free non-isocyanate poly (ester amide/urethane) networks with improved thermal stability on the basis of vegetable oils', *Polym. Degrad. Stab.*, vol. 155, pp. 111–121, Sep. 2018, doi: 10.1016/j.polymdegradstab.2018.07.010.

[13] M. Liu, B. Liu, L. Liang, F. Wang, L. Shi, and J. Sun, 'Design of bifunctional NH3I-Zn/SBA-15 single-component heterogeneous catalyst for chemical fixation of carbon dioxide to cyclic carbonates', *J. Mol. Catal. Chem.*, vol. 418–419, pp. 78–85, Jul. 2016, doi: 10.1016/j.molcata.2016.03.037.

[14] J. P. Burelbach, 'ADVANCED REACTIVE SYSTEM SCREENING TOOL (ARSST)', Orlando, Oct. 2000, p. 6.

[15] X. Lu, Y. Wang, L. Estel, N. Kumar, H. Grénman, and S. Leveneur, 'Evolution of Specific Heat Capacity with Temperature for Typical Supports Used for Heterogeneous Catalysts', *Processes*, vol. 8, no. 8, Art. no. 8, Aug. 2020, doi: 10.3390/pr8080911.

[16] C. (Charles) Paquot and A. Hautfenne, *Standard methods for the analysis of oils, fats, and derivatives*. Blackwell Scientific Publications, 1987.

[17] R. R. Jay, 'Direct Titration of Epoxy Compounds and Aziridines.', *Anal. Chem.*, vol. 36, no. 3, pp. 667–668, Mar. 1964, doi: 10.1021/ac60209a037.

[18] F. P. Greenspan and D. G. MacKellar, 'Analysis of Aliphatic Per Acids', *Anal. Chem.*, vol. 20, no. 11, pp. 1061–1063, Nov. 1948, doi: 10.1021/ac60023a020.

[19] F. Stoessel, *Thermal Safety of Chemical Processes: Risk Assessment and Process Design*. John Wiley & Sons, 2020.

[20] K. I. M. Al-Malah, *Aspen Plus: Chemical Engineering Applications*. John Wiley & Sons, 2016.

[21] K. Eränen, 'Abatement of Nitric Oxide by Catalytic Decomposition and Selective Catalytic Reduction with Hydrocarbons', Åbo Akademi University, 2004.

[22] A. J. Bonon, Y. N. Kozlov, J. O. Bahú, R. M. Filho, D. Mandelli, and G. B. Shul'pin, 'Limonene epoxidation with H2O2 promoted by Al2O3: Kinetic study, experimental design', *J. Catal.*, vol. 319, pp. 71–86, Nov. 2014, doi: 10.1016/j.jcat.2014.08.004.

[23] 'Mechanism of Al3+-Catalyzed Oxidations of Hydrocarbons: Dramatic Activation of H2O2 toward O−O Homolysis in Complex [Al(H2O)4(OOH)(H2O2)]2+ Explains the Formation of HO• Radicals | Inorganic Chemistry'. https://pubs.acs.org/doi/abs/10.1021/ic102476x (accessed Apr. 10, 2021).

[24] H. Haario, 'MODEST User's Manual'. Profmath Oy, Helsinki, 1994.

[25] L. Peña Carrodeguas *et al.*, 'Fatty acid based biocarbonates: Al-mediated stereoselective preparation of mono-, di- and tricarbonates under mild and solvent-less conditions', *Green Chem.*, vol. 19, no. 15, pp. 3535–3541, 2017, doi: 10.1039/C7GC01206C.

[26] D. Miloslavskiy, E. Gotlib, O. Figovsky, and D. Pashin, 'Cyclic Carbonates Based on Vegetable Oils', *Int. Lett. Chem. Phys. Astron.*, vol. 27, pp. 20–29, Feb. 2014, doi: 10.18052/www.scipress.com/ILCPA.27.20.

[27] L. Ruiz *et al.*, 'Upgrading castor oil: From heptanal to non-isocyanate poly(amide-hydroxyurethane)s', *Polymer*, vol. 124, pp. 226–234, Aug. 2017, doi: 10.1016/j.polymer.2017.07.070.

[28] M. Sankar, T. G. Ajithkumar, G. Sankar, and P. Manikandan, 'Supported imidazole as heterogeneous catalyst for the synthesis of cyclic carbonates from epoxides and CO2', *Catal. Commun.*, vol. 59, pp. 201–205, Jan. 2015, doi: 10.1016/j.catcom.2014.10.026.

[29] W.-H. Zhang *et al.*, 'Graphene oxide grafted hydroxyl-functionalized ionic liquid: A highly efficient catalyst for cycloaddition of CO2 with epoxides', *Appl. Catal. Gen.*, vol. 509, pp. 111–117, Jan. 2016, doi: 10.1016/j.apcata.2015.10.038.

[30] J. Sun, J. Ren, S. Zhang, and W. Cheng, 'Water as an efficient medium for the synthesis of cyclic carbonate', *Tetrahedron Lett.*, vol. 50, no. 4, pp. 423–426, Jan. 2009, doi: 10.1016/j.tetlet.2008.11.034.

[31] X. Zhou, Y. Zhang, X. Yang, J. Yao, and G. Wang, 'Hydrated Alkali Metal Halides as Efficient Catalysts for the Synthesis of Cyclic Carbonates from CO2 and Epoxides', *Chin. J. Catal.*, vol. 31, no. 7, pp. 765–768, Jul. 2010, doi: 10.1016/S1872-2067(09)60086-3.

[32] P. Mazo and L. Rios, 'Carbonation of Epoxidized Soybean Oil Improved by the Addition of Water', *J. Am. Oil Chem. Soc.*, vol. 90, no. 5, pp. 725–730, May 2013, doi: 10.1007/s11746-013-2214-3.

[33] J. Tharun, R. Roshan, A. C. Kathalikkattil, K. D. Heon, H. Mo, and D.-W. Park, 'Natural amino acids/H2O as metal- and halide-free catalyst system for the synthesis of propylene carbonate from propylene oxide and CO2 under moderate conditions', p. 8, 2012.

[34] M. Alves, B. Grignard, S. Gennen, C. Detrembleur, C. Jerome, and T. Tassaing, 'Organocatalytic synthesis of bio-based cyclic carbonates from CO $_2$ and vegetable oils', *RSC Adv.*, vol. 5, no. 66, pp. 53629–53636, 2015, doi: 10.1039/C5RA10190E.

[35] R. Luo, X. Zhou, W. Zhang, Z. Liang, J. Jiang, and H. Ji, 'New bi-functional zinc catalysts based on robust and easy-to-handle N-chelating ligands for the synthesis of cyclic carbonates from epoxides and CO2 under mild conditions', *Green Chem.*, vol. 16, no. 9, pp. 4179–4189, Aug. 2014, doi: 10.1039/C4GC00671B.